Fall 2014

# The role of microstructure on the combustion and impact behavior of mechanically activated nickel/aluminum reactive composites

Benjamin Aaron Mason
*Purdue University*

Graduate School Form 30
(Revised 08/14)

# PURDUE UNIVERSITY
## GRADUATE SCHOOL
## Thesis/Dissertation Acceptance

This is to certify that the thesis/dissertation prepared

By Benjamin Aaron Mason

Entitled
THE ROLE OF MICROSTRUCTURE ON THE COMBUSTION AND IMPACT BEHAVIOR OF MECHANICALLY ACTIVATED NICKEL/ALUMINUM REACTIVE COMPOSITES

For the degree of Doctor of Philosophy

Is approved by the final examining committee:

Steven F. Son

Lori J. Groven

Alejandro H. Strachan

I. Emre Gunduz

To the best of my knowledge and as understood by the student in the Thesis/Dissertation Agreement, Publication Delay, and Certification/Disclaimer (Graduate School Form 32), this thesis/dissertation adheres to the provisions of Purdue University's "Policy on Integrity in Research" and the use of copyrighted material.

Approved by Major Professor(s): Steven F. Son

Lori J. Groven

Approved by: Ganesh Subbaryan 10/16/2014

Head of the Department Graduate Program Date

# THE ROLE OF MICROSTRUCTURE ON THE COMBUSTION AND IMPACT BEHAVIOR OF MECHANICALLY ACTIVATED NICKEL/ALUMINUM REACTIVE COMPOSITES

A Dissertation

Submitted to the Faculty

of

Purdue University

by

Benjamin Aaron Mason

In Partial Fulfillment of the

Requirements for the Degree

of

Doctor of Philosophy

December 2014

Purdue University

West Lafayette, Indiana

For

Julia, Eldon, Lilly, and Riley

# ACKNOWLEDGMENTS

I would like thank my examining committee co-chairs, Prof. Steven Son and Prof. Lori Groven, and committee members Prof. Alejandro H Strachan, and Dr. I. Emre Gunduz for their critical guidance and support. Funding from the Defense Threat Reduction Agency (DTRA), grant number HDTRA1-10-1-0119 Counter-WMD basic research program, Dr. Suhithi M. Peiris, program director is gratefully acknowledged. Additional funding and support was provided by the William K. and Gail E. Cordier Fellowship. I would like to acknowledge Dr. Khachatur Manukyan, Tatyana Orlova, and Prof. Alexander Mukasyan of Notre Dame University for performing XRD, SEM, and TEM analysis. I would like to acknowledge Prof. Travis Sippel of Iowa State University for performing DSC/TGA/FTIR analysis. I would also like to acknowledge the suggestions of Dr. Abilash Nair and Prof. Alberto Cuitino of Rutgers University. In addition I would like to thank Matt Beason and Raghav Ramachandran for the assistance with experimental work and data analysis.

TABLE OF CONTENTS

Page

# LIST OF TABLES

# LIST OF FIGURES

Figure Page

Figure Page

# ABSTRACT

Mason, Benjamin Aaron Ph.D., Purdue University, December 2014. The Role of Microstructure on the Combustion and Impact Behavior of Mechanically Activated Nickel/Aluminum Reactive Composites. Major Professors: Steven F. Son and Lori J. Groven, School of Mechanical Engineering.

Metal-based reactive composites are a class of materials that consist of at least one metals, such as Ni/Al, that have high-energy densities and can produce significant energy output during exothermic reaction after thermal or mechanical initiation. However, conventionally these materials typically have slow reaction rates and are difficult to ignite at typical micron particle size ranges limiting their application. Therefore, mechanical activation techniques have been used to create materials with high surface areas and smaller characteristic dimensions in order to increase combustion velocity and ignition sensitivity. Their combustion and mechanical impact behavior is being studied to develop the understanding needed so that the materials can be ultimately developed for applications such as multi-functional energetic materials, blast enhancement and synthesis of novel metastable non-equilibrium materials.

In this work Ni and Al powder is mixed by High-Energy Ball Milling (HEBM) to produce a mechanically activated (MA) Ni/Al reactive composite. A two-step process is adopted that includes dry milling followed by wet milling using hexanes as a process control agent. The microstructure of the resulting powder contains layered Ni and Al laminates that have micron to nano-scale dimensions depending upon the dry milling time and particle size of the material. The mechanical impact response and combustion behavior of these materials was studied through a series of experiments.

Mechanical impact experiments were performed using a modified Asay shear experiment where properties such as mechanical impact ignition threshold, ignition delay time, and combustion velocity were identified. It was found that the mechanical

impact ignition threshold decreases as the dry milling time increases. The material with the longest dry milling time considered (97% $t_{cr}$ where $t_{cr}$ is the critical milling time that results in combustion during milling, which was 17.5 minutes, ignited at impact energy of $\sim$50 $J$ or higher (projectile speed of $\sim$65 $m/s$). Ignition delays due to the formation of hotspots ranged from 1.2 to 6.5 $ms$ and were observed to be in the same range for all milling times considered less than $t_{cr}$. Combustion velocities ranged from 25-31 $cm/s$ for impacted samples at an impact energy of 200-250 $J$.

Combustion experiments on MA Ni/Al pressed into cylindrical pellets shows that the combustion velocities increase as the milling time increases from $\sim$9.4 $cm/s$ at 25% ($t_{cr}$) to $\sim$20 $cm/s$ at a milling time of 97% $t_{cr}$. Maximum combustion temperatures were measured to be $\sim$1870 $\pm$ 35 $K$ for samples milled up to 50% $t_{cr}$, whereas combustion temperatures for materials milled for 97% $t_{cr}$ were on average of 100 $K$ lower. It was also shown that hydrocarbon contaminants are milled into the MA Ni/Al composite particles during the wet milling step and result in the expansion of the pellets during combustion. It was shown that the concentration of hydrocarbon contamination decreased as the dry milling times increased, which suggests particle structure and mechanical property evolution during dry milling also play a role in contamination during wet milling.

Mechanically activated Ni/Al composite powders were also annealed at two different temperatures to observe the effect of intermetallic formation and strain relaxation on the reaction kinetics. Williamson-Hall analysis suggests that recovery occurs at an annealing temperature of 403 $K$, resulting in lower strains for both Al and Ni. At an annealing temperature of 460 $K$, both recovery and Al grain growth was observed along with the growth of $NiAl_3$ phase, which was also detected using scanning electron microscopy. The morphology and characteristic laminate dimensions were not affected significantly by annealing. The 403 $K$ annealing had little effect on combustion velocities and temperature, but the 460 $K$ annealing significantly reduced the combustion velocities and temperatures. This shows that the combustion velocities

and temperatures are not significantly affected by strain relaxation but are largely influenced by the formation of $NiAl_3$ during annealing.

Lastly, it was shown that cleaning the milling jar with hexanes, as opposed to water, decreased the amount of cold-welding on the milling jar walls and media. This reduced the finial yield of fine particles ($<106\ \mu m$) and increased the concentration of solid solutions, and intermetallics. As a result of this loss in available heat release, combustion temperatures, and combustion velocities decreased.

# 1. INTRODUCTION

## 1.1 Motivation

Metal-based reactive powder composites, such as those consisting of nickel (Ni) and aluminum (Al), are a class of energetic materials that have high-energy densities and can produce significant heat release during reaction by thermal or mechanical initiation. Their potential use as structural energetic materials, as enhanced blast materials and for the synthesis of novel metastable non-equilibrium materials has driven research focused on their mechanical impact behavior [1–6]. However, these materials typically have slow reaction rates and are difficult to ignite at conventional micron particle size ranges limiting their application. Therefore, significant effort has been focused on creating materials with high surface areas and smaller characteristic dimensions in order to increase combustion velocity and ignition sensitivity. Reactive powder composites with these features have been fabricated by using nanopowders [3, 7–9], magnetron sputtering [10–15] and mechanical activation techniques [2, 4, 16–18]. Mechanical activation fabrication techniques are of particular interest, which increase combustion velocity and ignition sensitivity by modifying the system's morphology and mechanical properties through cold working. This is achieved by high-pressure collisions between the particles and the milling media in which the particles are simultaneously cold worked and cold welded together, resulting in composite particles. If milled for a long enough time, the individual components form stable intermetallic compounds. The milling time needed to completely react the material is termed the critical reaction time ($t_{cr}$). When milling is arrested prior to $t_{cr}$, composite particles are produced that consist of intermixed material with nano/microscale structures/laminates. Using a two step dry/wet milling procedure, Manukyan *et al.* [4] showed that composite particles milled for $\sim$25% $t_{cr}$ or less consist

primarily of structures/laminates intermixed on the micron scale, and as the milling duration increases, the ratio of nano to micron scale structures/laminates increases until the $t_{cr}$ and the material reacts. It has been shown that the intermixing of these materials at both the micron and nano scale increases thermal and impact sensitivity due to smaller diffusion distances and increased contact areas [2, 4, 17, 19–23]. However, the role and extent to which the modified microstructural properties affect combustion and mechanical impact behavior of these materials has yet to be fully investigated.

## 1.2 Objective

The objective of the work in this dissertation is to gain a better understanding of how the variation of microstructure properties, modified by parameters such as milling duration, annealing, and milling jar cleaning agents, influences the impact ignition, reaction propagation behavior, combustion temperatures and reaction kinetics of mechanically activated (MA) Ni/Al, so that a more comprehensive understanding of these systems can be gained along with data that can be used to validate and calibrate continuum and molecular dynamic models that are currently being developed in conjunction with this work [5, 24]. For this purpose MA Ni/Al composite powders were produced through high-energy ball milling. Mechanical impact experiments were performed to quantify the material's behavior under dynamic loading. Combustion experiments were performed to identify combustion velocities and temperatures. Mechanically activated Ni/Al composite powders have been annealed at different temperatures to determine the effect of phase formation and strain relaxation on their thermal response and combustion performance. Lastly the effect of water and hexane used during milling jar cleaning on resulting material yield, microstructure, and combustion behavior was assessed.

## 1.3 Organization

The work presented in this dissertation includes a series of four studies that investigate different aspects relating to the combustion or impact performance of MA Ni/Al reactive composites. Excluding Chapter 1 and 6, each chapter represents work that has been or will be published as a separate journal article and contains an introduction, experimental, results/discussion and conclusions section. In Chapter 2 the role of microstructure refinement modified via milling duration on the impact ignition and resulting reaction propagation will be discussed. Chapter 3 summarizes the role of microstructure refinement modified via milling duration on the deflagration behavior of pressed cylindrical compacts. Chapter 4 reports the effect of annealing on the combustion behavior of MA Ni/Al. Chapter 5 discusses how of water and hexane during milling jar cleaning can affect the resulting material yield and combustion behavior. Lastly in Chapter 6 a summary and conclusions of the research and the are presented.

# 2. THE ROLE OF MICROSTRUCTURE REFINEMENT ON THE IMPACT IGNITION AND COMBUSTION BEHAVIOR OF MECHANICALLY ACTIVATED NI/AL REACTIVE COMPOSITES

## 2.1 Introduction

Numerous experimental and theoretical studies have been published on impact behavior and shock compression of metal-based reactive powder mixtures with metals such as Al, Ni, Si, Ti, W, Nb, and more [1–3,6,16]. Yet the fundamental mechanisms that govern the initiation and front propagation are not well understood. For example, their energy release characteristics depend on the mode of initiation, and reaction propagation, in a currently unpredictable way. The lack of a predictive understanding of these materials leads to their underutilization and therefore significant effort is being dedicated to characterizing and modeling these reactions [1].

Two distinct modes for reaction upon impact have been identified, shock-assisted and shock-induced chemical reactions [25]. Shock-assisted reactions occur in the period of thermal equilibration typically well after the shock wave has passed. In contrast shock-induced reactions occur within or immediately after the pressure rise of the shockwave upon mechanical impact. Shock-assisted reactions occur due to heat generation from the compaction of the reactive material. This mechanical heating can be caused by plastic deformation, pore collapse, brittle fracture of particles, friction between particles, and shockwave interactions. Chemical reaction occurs following this mechanical dissipative heating. This reaction may continue and transition to a combustion wave, or quench.

In the regime of shock-assisted reactions it has been shown that most metal-based reactive composites, such as Ni/Al, require high impact energies in order to initiate a reaction [1, 26]. However, nanoscale reactive composites are significantly

more sensitive to impact and thermal ignition and have faster reaction rates than mixtures using micron size powders due to higher surface areas and smaller diffusion distances [3, 7, 27]. It has also been observed that higher bulk densities can lower impact ignition thresholds in nano mixtures [3]. In addition, material properties such as ductility and yield strength will also play a large role. For example, when the reactive composite W/Al is impacted, the ignition threshold is lower than that of Ni/Al. It was theorized that the lower ignition threshold of W/Al is due to the harder material (W) slicing through the more ductile material (Al) upon impact creating fresh interfaces and igniting the sample [3]. Therefore, for the W/Al reactive composite the energy needed to initiate reaction is acquired through both mechanical and thermal means where for the Ni/Al reactive composite the energy needed to initiate reaction is acquired mainly through thermal build up during the impact.

In addition to nanopowders, arrested reactive milling (ARM) or mechanical activation (MA) performed by high energy ball milling has been used to decrease the impact ignition of these materials [2,4,16]. Increasing the ignition sensitivities through MA occurs by changes in morphology, ductility and hardness through cold working. This is achieved by high energy collisions between the particles and milling media. When milling is arrested before the critical reaction time of a reactive mixture, such as Ni/Al, composite particles are produced that consist of intermixed material with structures/laminates on the micron to nanoscale. It has been shown that the intermixing of these materials on an intimate scale causes the observed increase in thermal and impact sensitivity due to smaller diffusion distances [2, 4, 17, 20–22]. However, the role and extent to which the modified microstructure properties have on compaction, ignition, and subsequent reaction propagation of impacted reactive powders has yet to be fully investigated and quantified.

A recent impact study using a rod-on-anvil Taylor impact test setup and small cylindrical samples of MA Ni/Al have indicated that milling duration affects ignition thresholds [2]. It was observed that material milled for 35% of the critical milling time ($t_{cr}$) had lower impact ignition thresholds than material milled for 65% $t_{cr}$, where

the $t_{cr}$ is the time at which reaction of the Ni/Al material would take place during milling if the milling is not arrested first. It was stated that this behavior is a result of competing effects of increased reactivity and increased strain hardening as the duration of milling increases [2]. This work, however, only investigated two milling durations and did not investigate combustion behavior upon reaction and therefore further work is required.

The objective of this work is to gain a better understanding of how the variation of microstructure, modified via milling parameters, influences the impact ignition and reaction propagation behavior of MA Ni/Al. With this information a more comprehensive understanding can be gained along with data that can be used to validate and calibrate continuum and molecular dynamic models that are currently being developed in conjunction with this work [5, 24].

## 2.2 Experimental

### 2.2.1 Mechanical Activation and Powder Characteristics

For this study 3-7 $\mu m$ Ni (Alfa Aesar) and -325 mesh Al (Alfa Aesar) were used to prepare an equiatomic MA Ni/Al reactive composite powder using a two-step dry and wet milling procedure as detailed in previous work [4]. In this method the Ni/Al was milled by high energy ball milling in a pure argon atmosphere using a PM100 (Retsch, Germany) planetary ball mill. The reactant powders were subjected to dry milling for different durations that include 4.25, 8.5, 12.75 and 17 minutes corresponding with roughly 25%, 75% and 97% of the critical milling time ($t_{cr}$) (when exothermic reaction occurs). This was done in 1-3 intervals consisting of upto 5 minutes of milling, followed by a 15 minutes rest to prevent excessive heating of the material. After dry milling the material was milled with hexane (98.5% hexane isomers, Mallinckrodt Chemicals) for a total of 10 minutes (two intervals of 5 minutes of milling, followed by a 15 minutes rest) with the same milling conditions, except that the jar was pressurized to $\sim$0.3 $MPa$. In all cases, the material was milled in a high purity (99.998%) Argon (Ar)

atmosphere. After wet milling the samples were dried in air for 1 hour (h) and then vacuum-dried at 300 $K$, for 24 h to remove any residual hexane. Once dry, the material was sieved into the particle size range of 25-53 $\mu m$ for further study.

Characterization of the resulting MA reactive composite powder was done by Dr. Manukyan at Notre Dame University and includes scanning electron microscopy (SEM), energy dispersive spectroscopy (EDS), scanning transmission electron microscopy (STEM), and by X-ray diffraction (XRD). Details of this characterization can be found in [4]. In summary, the milled Ni/Al powder consists of composite particles of intermixed Ni/Al having both course and fine microstructures. The course microstructure consists of Ni and Al intermixing with features on the micron-scale. Whereas, the material consisting of the fine microstructure consists of Ni and Al nanolaminate layers that are less than 30 $nm$ thick. Materials dry milled for 25% $t_{cr}$ or less consist primarily of course microstructure, materials dry milled for 50% and 75% $t_{cr}$ have a mixture of course and nanolaminate microstructures to varying degrees depending upon milling time and particle size. Material dry milled for 97% $t_{cr}$ consists of primarily the nanolaminate microstructure.

In this work, further characterization has been conducted to determine the heats of reaction of the MA Ni/Al as a function of milling time. This was done with a TA Instruments Q600 simultaneous thermo gravimetric analyzer and differential scanning calorimeter (TGA/DSC). In each experiment, $\sim$20 $mg$ of reactive material was heated at a heating rate of 10K/$min$ in an atmosphere of 99.9998% pure argon with flow rate of 100 $cm^3/min$ to 800 $K$.

### 2.2.2 Impact Experiments

Reaction initiation by mechanical impact was accomplished using the Asay shear experiment used previously with explosives [28] and other Ni/Al impact studies [4, 22, 27, 29]. The schematic of the experiments is show in Figure 2.1 MA Ni/Al power with a sieved particle size range of 25<d<53 $\mu m$ was compacted into square samples

with nominal dimensions of 20 $mm$ x 20 $mm$ x 2 $mm$ by applying a uniaxial pressure of 670 $MPa$. The compacts were pressed to a stop and a relative density in the range of 68-72% TMD was achieved. The compacted samples were placed into a specially designed holder equipped with an acrylic window for imaging the sample during the impact and subsequent reaction. A steel flyer plate press fit into a Delrin projectile (24 $g$ in total mass and 25.4 $mm$ diameter) was accelerated by means of a gas gun at a set velocity in the range of 50-220 $m/s$ or and impact energy of 30-600 $J$. The impact energy is simply the standard kinetic energy of the Delrin projectile. The projectile impacts a plunger inserted into a slot on the side of the sample holder. The plungers used had a flat impact face and had the same thickness and height of the MA Ni/Al compact. Impact experiments were recorded using a Phantom 7.3 high-speed camera at 50,000-88,000 frames per second (fps). Particle velocities and shock wave velocities of the of the sample upon impact were measured by marking the surface of the compacts with straight lines parallel to its impact edge and perpendicular to the impact direction. In addition to impact experiments, samples were also thermally ignited. Pressed samples were placed in the impact holder to maintain similar heat loss condition as the impact experiments. The samples were ignited with Nichrome wire with an ignition increment of about 75 $mg$ of loose MA Ni/Al powder placed on top of the sample. Burning rates were measured with a Phantom 7.3 high-speed camera at 3,000 fps.

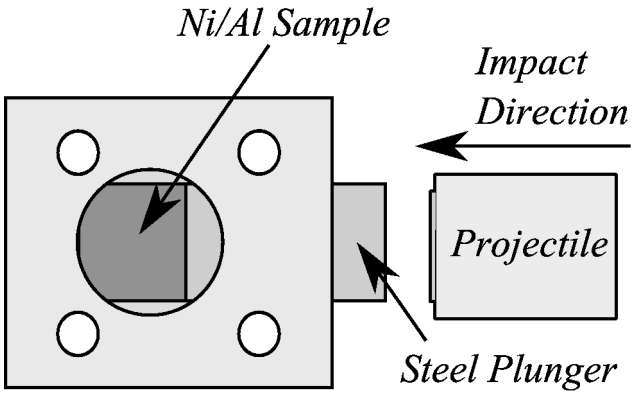


Figure 2.1. Schematic of pellet combustion experiment.

## 2.3 Results and Discussion

### 2.3.1 Impact Ignition Thresholds

To investigate how the impact ignition thresholds of shock-assisted reactions in MA Ni/Al are related to dry milling time and the thermal ignition thresholds, the MA Ni/Al material having a particle size of 25<d<53 $\mu m$ size was impacted as a function of milling time and impact energy. Figure 2.2 summarizes the experimental results as a function of dry milling time and impact energy on a Go, No-go basis (Go for a reaction ignition and No-go for no ignition). The ignition threshold was found to be between 160-200 $J$ (115-130 $m/s$) for material dry milled for 50% $t_{cr}$ and the lowest ignition threshold was identified to be between 40-60 $J$ (60-70 $m/s$) for material dry milled at 97% $t_{cr}$. The impact thresholds for MA Ni/Al milled for 25% $t_{cr}$ or less (including samples with no MA) could not be found as they did not react for the range of impact energies considered, even at the maximum experimental projectile speed of $\sim$200 $m/s$ (500 $J$). These results show that the impact ignition threshold decreases significantly between dry milling times of 25% $t_{cr}$ and 50% $t_{cr}$, corresponding to the appearance of nanolaminate microstructure. At milling times greater than 50% $t_{cr}$ the impact ignition threshold continues to decrease but more moderately, following a similar trend as the thermal ignition thresholds previously published [4]. This indicates that the sensitivity to impact ignition is directly correlated to the fraction of nanolaminate structure within the MA Ni/Al reactive composite, with the largest increase in sensitivity occurring with the initial formation of nanolaminate intra-particle microstructure.

These results are quite different than those reported by Herbold et al. [2], which showed a minimum ignition threshold for shorter milling durations (35% $t_{cr}$). These differences can be attributed to the type of impact experiment performed and the method of mechanical activation. The samples were impacted were using a rod-on-anvil Taylor impact experimental setup where the sample was unconfined resulting in rapid plastic deformation and then dispersion of the sample into the ambient envi-

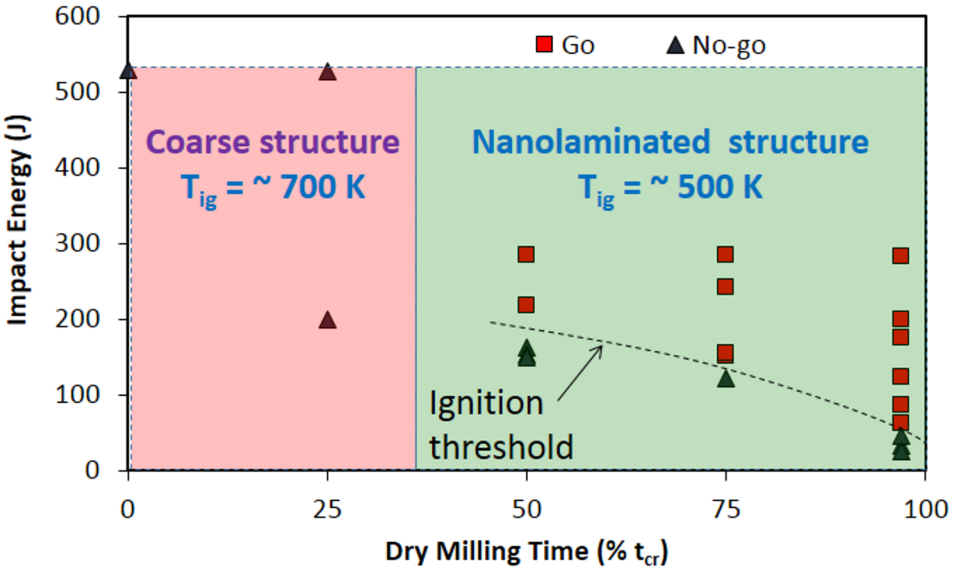


Figure 2.2. Impact reaction thresholds as a function of milling time and impact energy.

ronment. It was stated that rapid plastic deformation of the particles was the driving force that produced mechanical heating upon impact leading to ignition, which is why the material milled at 35% $t_{cr}$ had a lower impact threshold than the material milled at 65% $t_{cr}$ as the material milled for 35% $t_{cr}$ was expected to be more ductile. However, hardness measurements were not reported. In our work, the samples were confined during impact preventing particles from dispersing into the ambient environment. This configuration allows for heat generation over an extended time and the observation of delayed reactions. As a result sample ignition can be caused by heating during (e.g., plastic deformation) and after the impact (e.g., heating due to shock wave reflections or localized hot spot ignition). Differences in mechanical activation may also explain the observed differences as the properties of the MA of Ni/Al material will vary not only due to milling duration but also to other parameters such as, but not limited to, initial particle size, type of mill, and charge ratio. It has been shown that varying milling parameters such as the initial powder size, and the charge ratio results in significant differences in the resulting microstructure [17,30,31]

such as the Ni/Al laminate frequency and size, which will affect properties such as the materials ductility, heat of reaction, and will in-turn inevitably affect the impact ignition sensitivity also.

### 2.3.2 Hotspot Ignition

In a typical impact experiment at projectile velocities of 50-150 $m/s$ the plunger impacts the Ni/Al sample at an initial velocity of 35-100 $m/s$, respectively. This results in an impact energy of 30-280 $J$ and a lateral displacement of the plunger by about 4-9 $mm$ depending upon the impact velocity. Still images of a typical impact and subsequent reactions are shown in Figure 2.3 for the flat plunger cases. The first three images show the flat plunger impacting a MA Ni/Al sample with an impact energy of about 200 $J$ (130 $m/s$ projectile velocity). The total time of compaction was 0.14 $m/s$. The third image at t = 8 $ms$ shows the sample about 3 $m/s$ after the sample initially ignited, where t = 0 is the time at which the plunger is observed to begin to move. In this frame, 3 of 4 ignition locations or hotspots are visible. The first luminescent hotspot appeared at about t = 5.4 $m/s$ followed by ignition of other hotspots at various locations, the last of which ignited at t = 11.2 $m/s$. The combustion front propagation (right to left) is seen at times t = 20 $m/s$ and t = 40 $m/s$ in the last two images of Figure 2.3. The hotspot ignition was identified by the commencement of a luminous combustion front from a specific point. It was observed that for impact experiments using the flat plunger, ignition typically occurred by hotspot formation in 2-5 locations at the plunger-sample interface, along the upper and lower edges of the compact and occasionally within the bulk of the sample.

The ignition delays, defined by the time at which the first luminous hotspot appeared after impact that was followed by combustion propagation, are show in Figure 2.4. The ignition delays for MA Ni/Al compacts impacted at impact energies of 200-250 $J$ (projectile velocities of 130-145 $m/s$) ranged from about 1.2 to 6.5 $ms$. In Table 2.1 hotspot ignition times for each hotspot observed during an experiment are

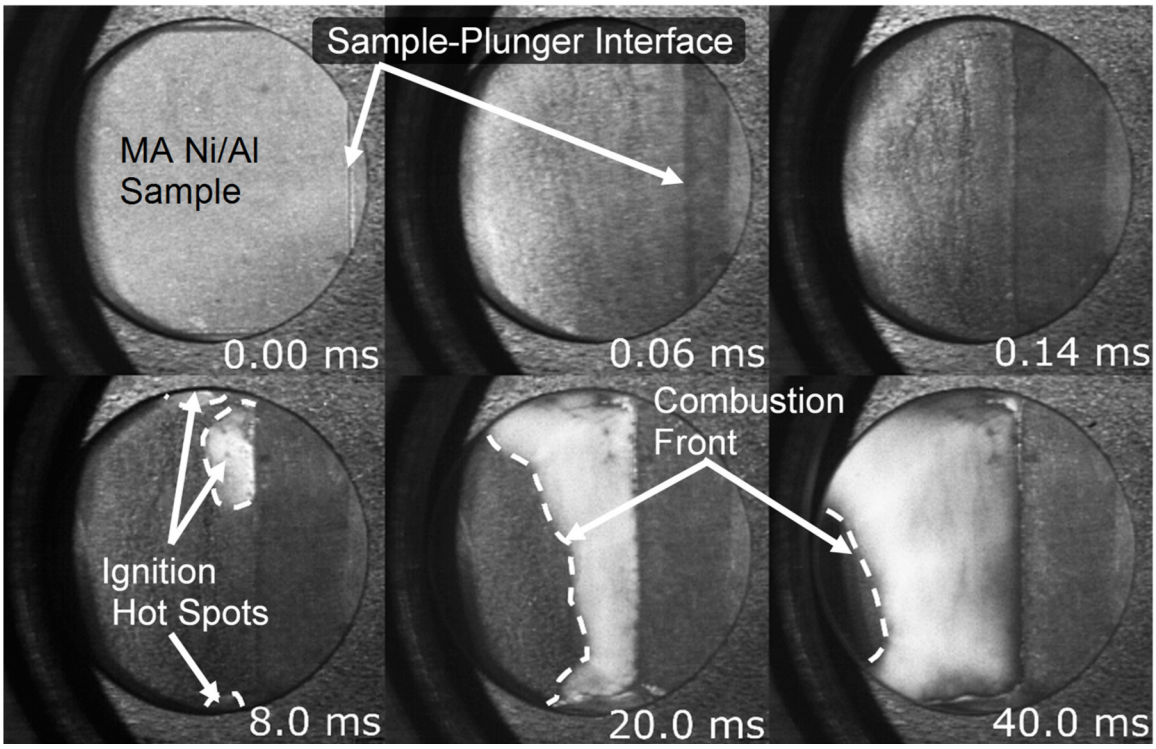


Figure 2.3. Impact ignition and reaction of MA Ni/Al compacts using a flat plunger.

shown for 2-3 samples for each milling time. The hotspot ignition delays ranged from about 1.2 to 15 $ms$.

All the samples were impacted at roughly the same conditions and therefore the heat generation upon impact is very similar for each case. Consequently, it could be expected that the samples with higher thermal ignition thresholds (i.e., shorter milling times) would have longer ignition delays due to the length of time that is required for the temperature to reach the thermal ignition threshold temperature after impact. However, this trend was not clearly observed. The results do show that the earliest ignition delay was measured for a sample dry milled for 97% $t_{cr}$, followed by 75% $t_{cr}$, and then 50% $t_{cr}$. However, the longest ignition delays were also measured for the material milled for 97% $t_{cr}$. It appears that the ignition delays are not strongly dependent upon milling time as long as the material is milled for at least 50% $t_{cr}$ and

that the variability in ignition delays observed is simply the intrinsic variability of the experiment. The variability does seem to increase as the critical milling time is reached, but the reason for that is unclear.

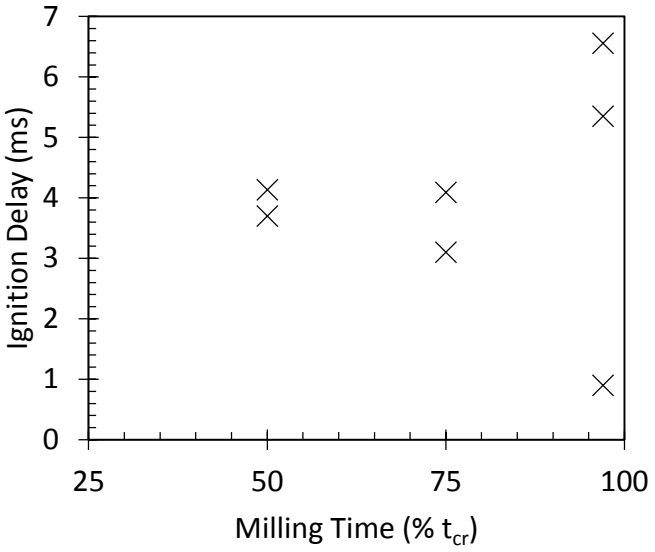


Figure 2.4. Ignition delay times for MA Ni/Al samples impacted at with an impact energy of 200-250 $J$ (130-145 $m/s$).

Table 2.1. Hotspot ignition delay times for MA Ni/Al samples as a function of milling time that were impacted at with an impact energy of 200-250 $J$ (130-145 $m/s$). Each impact experiment exhibits 2-5 hotspot ignition points.

| | Hotspot Ignition Times ($ms$) | | |
|---|---|---|---|
| Sample | 50% $t_{cr}$ | 75% $t_{cr}$ | 97% $t_{cr}$ |
| 1 | 3.7, 3.8, 3.9, 4.5 | 3.1, 4.1, 7.0, 8.8, 9.4 | 6.5, 10.6, 12.6 |
| 2 | 4.1, 10.7 | 4.1, 11.1, 8.6, 8.8 | 1.2, 5.0, 15.5 |
| 3 | | | 5.4, 6.7, 7.1, 11.16 |

### 2.3.3 Combustion Velocities

As previously shown in Figure 2.3, upon ignition the reaction fronts were seen to propagate through the sample originating from the hotspot locations. Based on the microstructure characterization it might be expected that combustion velocities would increase as a function of milling time due to an increased concentration of nanolaminate microstructure (decrease in diffusion distances) and lower reaction thresholds [4], however this was not observed. For both thermally and impact ignited cases the combustion velocities did not vary significantly as a function of dry milling time for those considered. It should be noted that Ni/Al with no MA at 70% TMD would not ignite without substantial preheating, nor would it ignite upon impact for the impact energies considered. For MA Ni/Al compacts thermally ignited within the sample holder the average combustion velocities were measured to be between 21-23 $cm/s$ (see Figure 2.5). In comparison, combustion velocities ranged from 25-31 $cm/s$ for samples impacted with at an impact energy of 200-250 $J$. In Figure 2.5 the average combustion velocity and the range of velocities observed is reported. The increase in combustion velocity for the impacted samples as compared to the thermally ignited samples is due to a higher packing density and to an increased initial temperature as a result of the impact. Both of these conditions have been shown to increase the combustion velocity of the Ni/Al reaction [16, 32].

The observed combustion velocities are also much faster than previously reported for both milled and unmilled Ni/Al reactives with micron sized powders. Taking into account both loose powder mixtures and cold-pressed compacts, typical combustion velocities have been reported to be on the order of 1-12 $cm/s$ [16, 33]. Recently Bacciochini et al. [16] reported combustion velocities for thermally ignited MA Ni/Al compacts cold-pressed to 40-80% TMD in the range of 3-6 $cm/s$. The combustion velocities in this work are 4-10x faster than those. However, the milling procedure utilized by Bacciochini et al. [16] varied significantly from that of this work. In their work the critical dry milling time was between 38-42 $min.$, whereas the critical milling

time for this work is between 17-17.5 $min$. Therefore, the resulting microstructures would vary between them. Different microstructures result in different combustion velocities because parameters such as laminate size, laminate frequency, defect density and inter-particle porosity will change as the milling parameters are changed [17, 31, 34]. All of these factors play a role in the resulting combustion velocities of these materials.

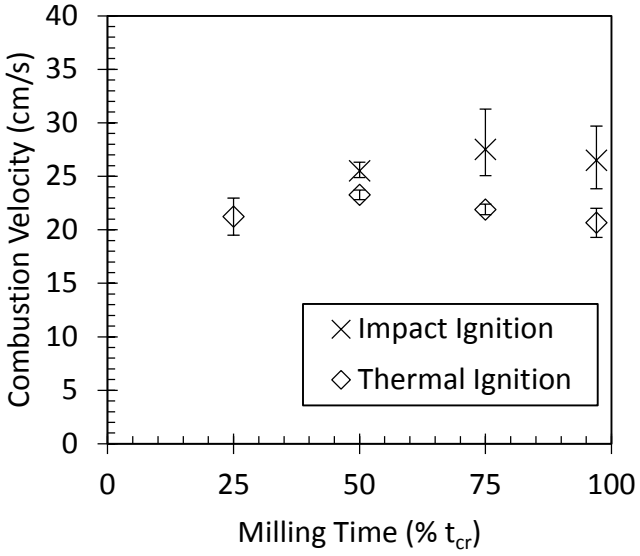


Figure 2.5. Average combustion velocity of MA Ni/Al samples thermally ignited and impacted with an impact energy of 200-250 $J$ (130-140 $m/s$).

### 2.3.4 Thermal Analysis

DSC analysis of the MA Ni/Al material dry milled for 25% $t_{cr}$ and 97% $t_{cr}$ indicates that in the temperature range of 450 $K$ to 850 $K$ the materials react and exhibit three exothermic peaks before the melting point of Al [4]. DSC analysis of material dry milled for 50% $t_{cr}$ and 75% $t_{cr}$ show the same trend (see Figure 2.6). As the milling time increases the reaction onset temperatures and exothermic peaks shift to lower temperatures by 25-80 $K$ as compared with material dry milled for

25% $t_{cr}$. Previous work has shown that the decrease in sensitivity to thermal and mechanical impact is largely dictated by the temperature needed to begin the initial exothermic reaction (peak A) [4, 30, 34]. The exothermic reaction of peak A is due to the release of stored free energy, the initial dissolution of nickel into aluminum, and the formation of $NiAl_3$ [4, 30, 34], where the stored free energy is acquired by the formation of microdeformations (vacancies and dislocations) and amorphous Al during the milling process [30, 34, 35]. It is largely due to the introduction and increase in concentration of these components that results in the decrease of temperature needed to initiate the Ni/Al reaction [34]. Recent work has shown the initial formation of microdeformations and amorphous Al can occur at milling times starting at about 15% $t_{cr}$ [34]. This is supported with these DSC results and thermal ignition experiments [4] as ignition temperatures are significantly less than typical Ni/Al ignition temperatures (about 913 $K$). However, the lower temperature needed to initiate the initial exothermic reaction (peak A) reaches a minimum at a milling time of 50% $t_{cr}$. It is also at this milling duration that the initial formation of nanolaminate structures is detected.

As shown in 2.2 the exothermic reaction onset temperature for peak A is about 479 $K$ for a dry milling time of 25% $t_{cr}$ and then it lowers to about 460 $K$ and does not change significantly for dry milling times $\geq$ 50% $t_{cr}$. In addition to the reaction onset temperature, it is also between the milling times of 25% $t_{cr}$ and 50% $t_{cr}$ that the thermal ignition threshold lowers from about 660 $K$ to 590 $K$ and the mechanical impact ignition threshold lowers from an impact energy of greater than 500 $J$ (200 m/s) to about 200 $J$ (130 $m/s$). The increase reaction sensitivity between the milling times of 25% $t_{cr}$ and 50% $t_{cr}$ is likely due to a combination of increases in the concentration of microdeformations, amorphous Al and to the initial formation of nanolaminate structures in the MA Ni/Al material. Further milling beyond 50% $t_{cr}$ continues to increase the fraction of nanolaminate material and the thermal and impact ignition thresholds also decrease, however to a lesser extent.

With the decrease in thermal ignition temperatures there is also a loss in energy, the heat of reaction for the combined reaction of peak B and C changes significantly as a function of milling time (see Table 2.2). Between the milling times of 25% $t_{cr}$ and 50% $t_{cr}$ the heat of reaction for the combined reaction of peak B and C decreases significantly from 515 $J/g$ to 154 $J/g$, respectively. As the dry milling time is increased from 50% $t_{cr}$ to 97% $t_{cr}$ the magnitude and peak temperature of peak B remains unchanged but the third peak continues to shift to a lower temperature while its magnitude decreases resulting in a slightly lower heat of reaction for the combined reaction (peaks B and C). This indicates that an optimum milling time could be found where the sensitivity to thermal and mechanical impact is greatly increased and the loss of energy due to increased milling is minimized. For this system and milling method, the optimum dry milling time is in the range 50-75% $t_{cr}$.

This loss in energy in peaks B and C is potentially caused by the formation of intermediate Al/Ni phases formed during milling, however, different phases were not detected in unreacted material for any of the dry milling times considered [4], which could indicate the presence of amorphous intermediate Al/Ni phases or solid solutions. Further XRD analysis of samples annealed to 690 $K$ (dry milling time of 25% $t_{cr}$) or 620 $K$ (dry milling times of 50% $t_{cr}$ to 97% $t_{cr}$) show that the dominate phases present just after the reaction of Peak B are Ni, $NiAl_3$, and $Ni_2Al_3$ regardless of the milling time. It has previously been shown that material annealed to just after peak C (770 $K$) consist only of the phases Ni, $Ni_2Al_3$ and NiAl and material annealed to 1070 $K$ consisted of mainly NiAl regardless of whether the material dry milled for 25% $t_{cr}$ or 97% $t_{cr}$.

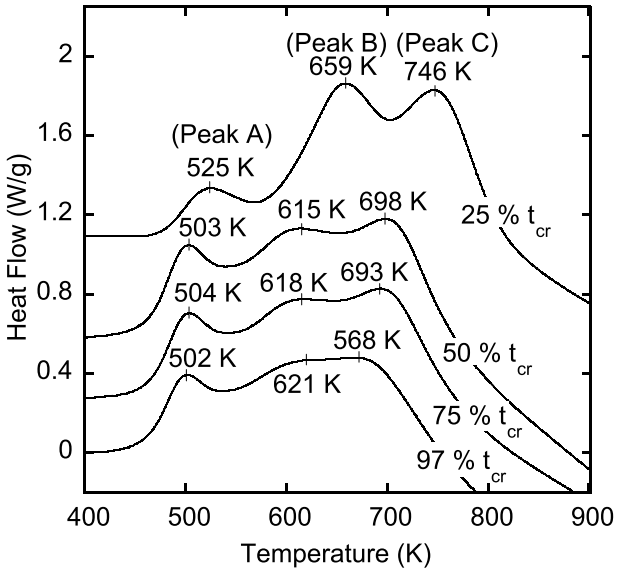


Figure 2.6. DSC traces for MA Ni/Al as a function of milling time.

Table 2.2. Reaction onset temperatures and heat of formation for acquired DSC traces.

| | Peak A | | Peak B-C | |
|---|---|---|---|---|
| Dry Milling time ($\%\ t_{cr}$) | Onset Temperature ($K$) | Heat of Reaction ($J/g$) | Onset Temperature ($K$) | Heat of Reaction ($J/g$) |
| 25 | 479 | 41 | 592 | 515 |
| 50 | 463 | 52 | 558 | 154 |
| 75 | 463 | 54 | 558 | 153 |

## 2.4 Conclusions

In summary, our experiments show that refining the microstructure of MA Ni/Al reactive composites by varying the dry milling time significantly affects the mechanical impact ignition threshold and resulting combustion behavior. For dry milling times of 0-25% $t_{cr}$ the impact ignition thresholds are greater than at least 500 $J$ (200 $m/s$) and as the milling time increases to 50% $t_{cr}$ the impact ignition threshold reduces to ∼200 $J$ (130 $m/s$). Further milling reduces the impact ignition threshold to ∼40-60 $J$ (60-70 $m/s$) as the total dry milling time increases from 50% $t_{cr}$ to

97% $t_{cr}$. High velocity imaging also showed that ignition of the sample occurred at ignition spots typically on or near the impact face and edges of the sample. Ignition delays were found to be on the order of 1-6.5 $ms$ and combustion velocities were on the order of 25-31 $cm/s$. Increased milling had little effect on the ignition delays or combustion velocities as long as the material was dry milled to at least 50% $t_{cr}$. Combustion velocities for compacts that were thermally ignited were in the range of 21-23 $cm/s$ for milling times of 25-75% $t_{cr}$, while unmilled materials did not propagate unless preheated for the densities considered. These results along with DSC analysis indicate that i) the driving mechanism behind reaction upon impact for these experiments is the rapid increase in temperature at localized hot spots on or near the impact face and edges of the sample and that when the hotspots reach the thermal ignition threshold, the impacted sample ignites and ii) that although increasing the milling time to near the critical milling time may reduce the thermal and impact ignition thresholds, the reductions are modest beyond a point and may not be worth the loss in reaction energy due to further milling. Here we find that the largest jump in sensitivity is between the dry milling times of 25% $t_{cr}$ and 50% $t_{cr}$ corresponding to when nanolaminate structures are initially detected during the ball milling process. Thermal analysis along with previous work indicates that the increase in the sensitivity to thermal and mechanical impact is dictated by a combination of three coupled factors: the formation of microdeformations (vacancies and dislocations), amorphous Al, and nanolaminate structures, which reduce the temperature needed to begin the dissolution of nickel into aluminum. DSC analysis showed that between the dry milling times of 25% $t_{cr}$ and 50% $t_{cr}$ the onset of the dissolution of nickel into aluminum shifted from 479 $K$ to 462 $K$. Further dry milling of the MA Ni/Al does not reduce the onset of the dissolution of nickel into aluminum but it does reduce the total energy output of the system, indicating that for this system and method a milling time of about 50-75% $t_{cr}$ is likely optimal when taking into account both the increased ignition sensitively of mechanical activation and potential loss in reaction energy with longer milling times.

# 3. THE EFFECT OF MICROSTRUCTURE REFINEMENT ON THE DEFLAGRATION BEHAVIOR OF MECHANICALLY ACTIVATED NI/AL COMPOSITES

## 3.1 Introduction

Mechanical activation techniques are of particular interest, as they can increase combustion velocities and ignition sensitivities by modifying the systems morphology and mechanical properties through refinement and cold working. This is achieved by high-pressure collisions between the particles and the milling media in which the particles are simultaneously cold worked and welded together, resulting in composite particles. If milled for a long enough time, the individual components form final stable intermetallic compounds. The milling time needed to completely react the material is termed the critical reaction time ($t_{cr}$). When milling is arrested prior to $t_{cr}$, composite particles are produced that consist of intermixed material with nano/microscale structures/laminates. Using a two step dry/wet milling procedure, Manukyan *et al.* [4] showed that composite particles milled for $\sim$25% $t_{cr}$ or less consist primarily of structures/laminates intermixed on the micron scale, and as the milling duration increases nanoscale laminates from, and the ratio of nano to micron scale structures/laminates increases until $t_{cr}$ is reached and the material reacts. It has been shown that the intermixing of these materials at both the micron and nano scale increases thermal and impact sensitivity due to smaller diffusion distances and increased contact areas [2, 4, 17–23]. However, the role and extent to which the modified microstructural properties affect the reaction velocity and combustion temperature has yet to be fully investigated. Initial work involving mechanically activated (MA) Ni/Al has focused on the 3Ni/Al system. Korchagin *et al.* [30, 35] reported combustion velocities that ranged from $\sim$0.1 to 1.4 $cm/s$ depending upon the milling time and milling energy.

The combustion velocities initially increased with extended milling until a threshold was reached. With further milling beyond the threshold, the combustion velocities would decrease due to poisoning or the formation of Ni/Al intermediates and solid solutions during milling. Combustion temperatures ranged from ∼850 to 1070 $K$ and followed the same trend as the combustion velocities. Under different milling conditions and with pressed samples, Hadjiafxenti *et al.* [20,36] reported combustion velocities that ranged from ∼0.9 to 5 $cm/s$, which increased with the pellet density due to enhanced thermal contact [20]. When compared to non-milled samples these studies show a slight increase in combustion velocities under analogous conditions [37]. As compared to non-milled samples significant increases in combustion velocities have been observed for the more exothermic equiatomic MA Ni/Al system. For material milled to ∼90% $t_{cr}$, Bacciochini *et al.* [16] reported combustion velocities that increased with compaction density from ∼3 $cm/s$ to 6 $cm/s$. These samples were cold-pressed to densities of ∼42 to 75% of the theoretical maximum density (TMD) respectively. Bacciochini *et al.* [16] were also able to achieve compaction densities of ∼99% through cold spray techniques. Combustion velocities of up to ∼24 $cm/s$ were reported for those compacts. Using low energy ball milling, Hadjiafxenti *et al.* [19] reported combustion velocities that were on the order of 20-24 $cm/s$ and ∼14 $cm/s$ for material milled for ∼87% $t_{cr}$ and ∼95% $t_{cr}$, respectively for pellets pressed at 68% TMD. Depending on compact density and pre-heat temperatures, combustion velocities of typical non-milled Ni/Al pellets are on the order of 1-12 $cm/s$ [32,33,38] for micron-sized powders. These studies show a significant increase in combustion velocities as compared to similar non-milled Ni/Al pellets. However, for MA Ni/Al, studies demonstrating the effects of microstructure on combustion are limited [16,19]. A full study investigating how varying microstructure refinement via milling duration affects the combustion behavior of equiatomic MA Ni/Al has not been done. The objective of this work is to characterize how the variation of microstructure, modified via dry milling duration, influences the combustion velocity and temperature of pressed, equiatomic MA Ni/Al reactive composite powders. With this information

a more comprehensive understanding of these materials can be gained along with data that can be used to develop continuum and molecular dynamics models that are currently being developed in conjunction with this work [5, 24].

## 3.2 Experiential

### 3.2.1 Mechanical Activation

For this work the mechanical activation procedure used was the same as in section 2.2.1.

### 3.2.2 Combustion Experiments

Combustion experiments were performed on cylindrical pellets of sieved (25 to 53 $\mu m$) Ni/Al particles that were pressed to 70% ± 2% TMD with a height 13.5 ± 0.2 $mm$ and a diameter of 12.7 $mm$. Figure 3.1 shows the schematic of the experiment. The pellets were thermally ignited to measure burning rates and combustion temperatures. To ensure consistent ignition and to promote a planar combustion front, the samples were ignited using a hot wire and ignition increment that ignited a 2 $mm$ thick compact of 97% $t_{cr}$ MA Ni/Al pressed at 65% ± 2% TMD. The 2 $mm$ compact would subsequently ignite the experimental sample. The ignition increment was A1A, a pyrotechnic igniter with a composition of (65 wt.-% Zr, 25 wt.-% Fe2O3 and 10 wt.-% diatomaceous earth). The combustion experiments were visually recorded using a high speed color Phantom v7.3 camera at a frame rate of 1000 frames/s (fps). Temperature measurements were taken with a FLIR series SC2500 infrared (IR) camera at 1000 fps and an Omega Type B (platinum/rhodium with 0.20 $mm$ dia.) thermocouple. The thermocouple was inserted in a ∼0.5 $mm$ x 0.6 $mm$ diameter hole, drilled 4 $mm$ from the top of the pellet. For repeatability, three separate experiments were conducted for each experimental condition.

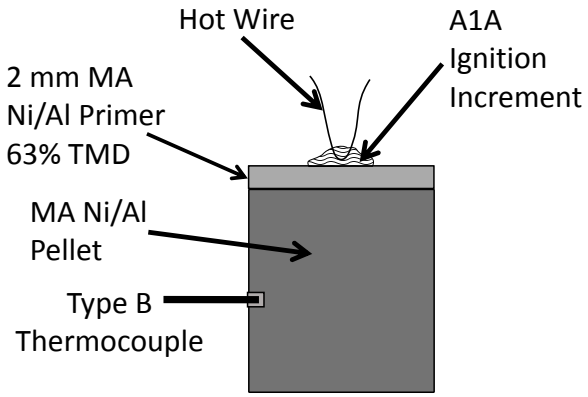


Figure 3.1. Schematic of pellet combustion experiment.

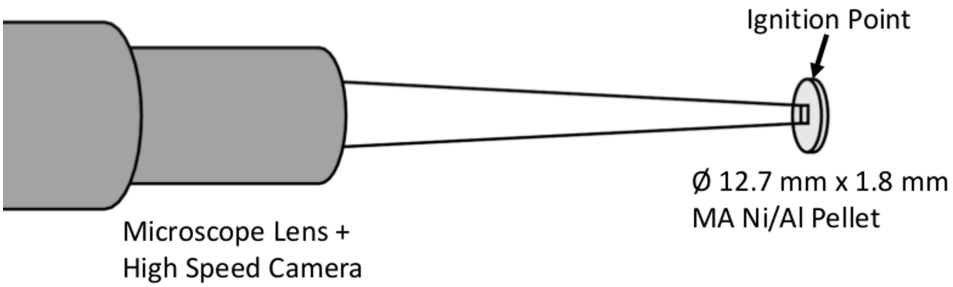


Figure 3.2. Schematic of combustion experiment using long distance microscopic optic.

### 3.2.3 Microscopic Observation Combustion Experiments

A second set of combustion experiments were performed in order to observe the flame front propagation on a microscopic scale. This was done using 12.7 $mm$ diameter cylindrical pellets with a height 1.8 $\pm$ 0.05 $mm$ that were pressed to 70% $\pm$ 2% TMD. Experiments were performed with sieved material in the size range of 106 to 355 $\mu m$ so that individual particles could be observed. A schematic of the experiment is shown in 3.2. A pellet was supported vertically using a pair of tweezers

and was ignited on one edge with a small butane torch. The reaction front was captured near the center of the pellet using the high speed video camera equipped with a long distance microscopic optic (Infinity Photo-Optical, K2 lens) at 1000 fps. The pixel resolution was 8 $\mu m$/pixel. The sample was illuminated with a focused, 1000 W Xenon arc lamp source (Newport Corp. #66921).

### 3.2.4 Product Characterization

Reacted pellets were analyzed using optical microscopy and X-ray diffraction (XRD) analysis. The reacted pellets were cross-sectioned, polished, and imaged with a Hirox digital microscope (Model # KH-8700) using an OL-140 II lens (140 - 1400x magnification). The prepared samples were then analyzed by XRD using a Bruker D8 Focus with a LYNXEYE detector operated at a scan speed of 5 $deg/min$ for the angular range of 20-120° ($2\theta$).

### 3.2.5 Thermal Analysis and Gas Phase Product Characterization

Evolved gas analysis was conducted using simultaneous differential scanning calorimetry and thermogravimetric analysis (DSC/TGA) coupled with a Fourier transform infrared (FTIR) spectrometer. Experiments were conducted on 20 ± 0.3 mg samples of as-milled Ni/Al using a Netzsch Jupiter F1 DSC/TGA with platinum furnace. The samples were heated from room temperature to 1073 $K$ at heating rate of 10 $K$/min under a steady flow of 20 mL/min of ultra high purity argon (99.999 vol.%). Prior to starting experiments, the instrument furnace was evacuated and backfilled with purge gas three times. The instrument exhaust was coupled to the cooled, external MCT detector of a Bruker Tensor 37 FTIR spectrometer using a Bruker TGA-IR light pipe and 200 C heated capillary transfer line. During DSC/TGA experiments, IR data was recorded every ∼3 C with a spectral resolution of 2 cm-1. Data was post-processed using Bruker Opus and Netzsch Proteus software. Additional but similar experiments

were run without FTIR using a TA Instruments Q600 TGA/DSC in order to more accurately measure weight loss.

## 3.3 Results and Discussion

### 3.3.1 Combustion Velocities

Increasing the dry milling time resulted in an increase in the combustion velocities of thermally ignited pellets from $9.4 \pm 0.2$ to $19.3 \pm 2.3$ $cm/s$ as shown in Figure 3.3 for materials milled for 25% $t_{cr}$ and 97% $t_{cr}$ respectively. The increase in combustion velocities with dry milling time is likely a result of the increase in the relative amount of nanolaminate structures formed through extended milling [4]. The observed combustion velocities are much faster than non-milled Ni/Al mixtures with micron sized powders, which are on the order of 1-5 $cm/s$ for cold-pressed compacts [32, 33, 38] at densities of 60% TMD and ignition at 70% TMD was only possible with substantial preheating.

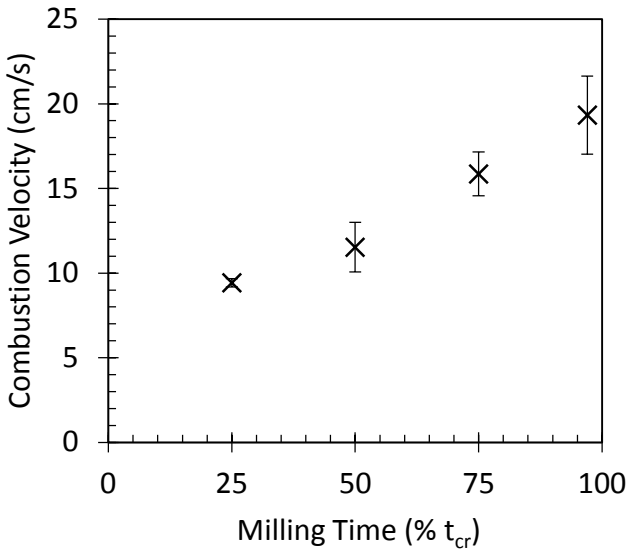


Figure 3.3. Combustion velocities of Ni/Al compacts as a function of dry milling time. Error bars indicate the standard deviation of at least 3 experiments.

The measured combustion velocities are comparable to previously reported velocities for MA Ni/Al at 1:1 ratio [16, 19], but they do not follow the same tend as the milling time approaches the $t_{cr}$. In past work with the 3Ni/Al system others [30, 35] and the Ni/Al system [19], it was observed that the combustion velocities initially increased with extended milling until a threshold was reached and then decrease as the milling duration approached the $t_{cr}$. The combustion velocity decrease is a result of the formation of Ni/Al intermediates and solid solutions during milling. In this work, a reduction in the combustion velocities at milling times close to the $t_{cr}$ were not observed, however a slight decrease in temperature was.

### 3.3.2 Combustion Temperatures

Figure 3.4 shows the temperature profile as measured by the IR camera and thermocouple as function of time for a typical burn measured 4 $mm$ from the top of the pellet. For this these experiments the emissivity was found to be range in of 0.90-0.95 when fitting the IR measurements to the maximum temperature and initial cooling of the temperature profile of the thermocouple. Upon ignition of the main pellet the reaction front travels down the pellet with an initial reaction temperature in the range of 1550-1790 $K$ depending upon the sample and milling time. After the reaction front passes it takes on average about 0.7 $\pm$ 0.3 s for the pellet to reach its maximum combustion temperature. The time to reach the maximum temperature was not observed to be a function of milling time.

Figure 3.5 shows the maximum combustion temperatures measured by IR as a function of milling time assuming an emissivity of 0.925. Due to the product expansion, thermocouple measurements were not feasible on samples milled for 25% and 50% $t_{cr}$. The average maximum combustion temperatures decreased from 1873 $\pm$ 30 $K$ (25% $t_{cr}$) to 1786 $\pm$ 30 $K$ (97% $t_{cr}$). The standard deviation of the maximum temperatures, however, increased dramatically from $\sim$10 $K$ (25% and 50% $t_{cr}$) to $\sim$80 $K$ (97% $t_{cr}$). The decrease in temperature is likely due to the formation of small

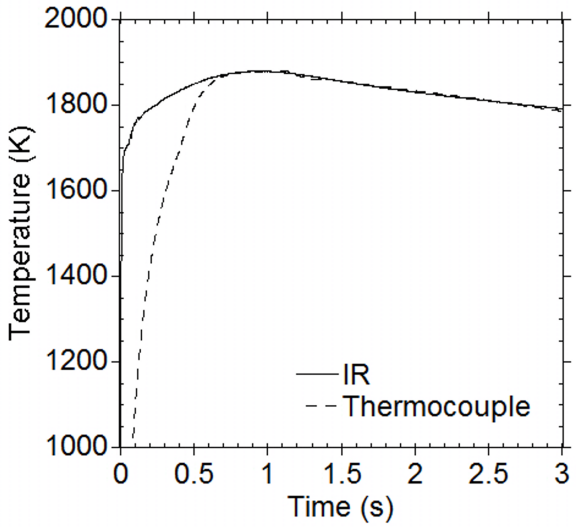


Figure 3.4. Combustion temperature profile of a typical Ni/Al pellet measured with IR camera and thermocouple. The best fit was at an emissivity of 0.9.

amounts intermediate and solid solution phases during milling. The larger deviation in in the material milled for 97% $t_{cr}$ is likely due to slightly varying amounts of intermediate and solid solution phases present in each pellet, which would likely become more significant at longer milling times. The decrease in combustion temperature, along with the increase in combustion velocities indicates that the increased microstructure refinement associated with increased milling duration has a larger effect on combustion velocities than energy loss due to the small amount intermediate phases formed during milling for this milling process.

### 3.3.3 Combustion Product Characterization

#### X-Ray Diffraction

X-Ray diffraction analysis of cross-sectioned samples did not show any phases other than NiAl for all of the milling times studied (see Figure 3.6). This is expected as the combustion temperatures close to the adiabatic combustion temperature of

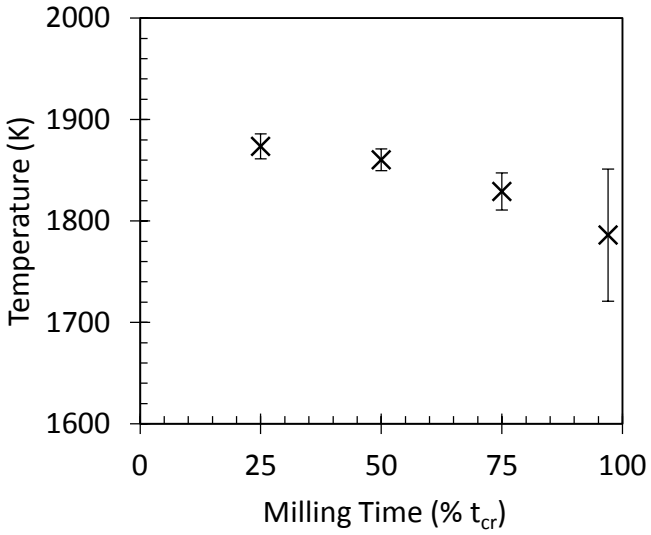


Figure 3.5. Maximum combustion temperatures of Ni/Al pellet as a function of dry milling time assuming an emissivity of 0.925. Error bars indicate the one standard deviation and the uncertainty due to emissivty is $\pm$ 30 $K$.

the system (1911 $K$) [39]. While not detected, it is also expected that some oxides formed as the pellets were burned in air.

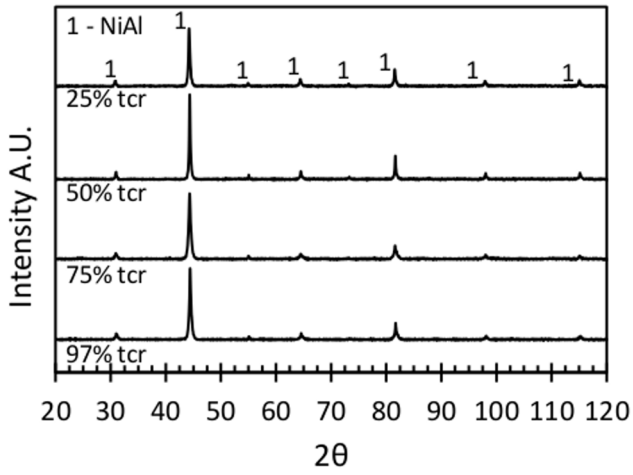


Figure 3.6. XRD results for thermally ignited MA Ni/Al pellets.

### Product expansion

Upon ignition of the main MA Ni/Al pellet by the primer pellet, a planar reaction front propagates down the pellet. Immediately following the reaction front, the sample expands axially in the direction opposite the reaction front propagation direction as shown in Figures 3.7 A. This expansion varied significantly as a function of milling time. Figure 3.8 shows a side-by-side comparison of the pellets after combustion for each milling time. For short milling times (25-50% $t_{cr}$), the pellet elongation during combustion was between 30 to 75% (Figure 3.9). Occasionally, the pellets would break apart due to the formation large voids. Expansion was less significant at longer dry milling times (10% for 75 and 97% $t_{cr}$) and nearly retained their original shape. Microscope images of cross-sectioned combustion products (see Figure 3.10) show that in all cases, pore sizes range from 1 $\mu m$ to ~80 $\mu m$, but for 25% $t_{cr}$, very large pores of up to several millimeters in length were formed within the pellet. For the 50% $t_{cr}$ dry milled samples, the largest pore sizes observed were up to 1 $mm$ in length. While some expansion [38] was expected due to the impurities, such as moisture or hydrocarbon residues, the drastic decrease as a function of dry milling was not.

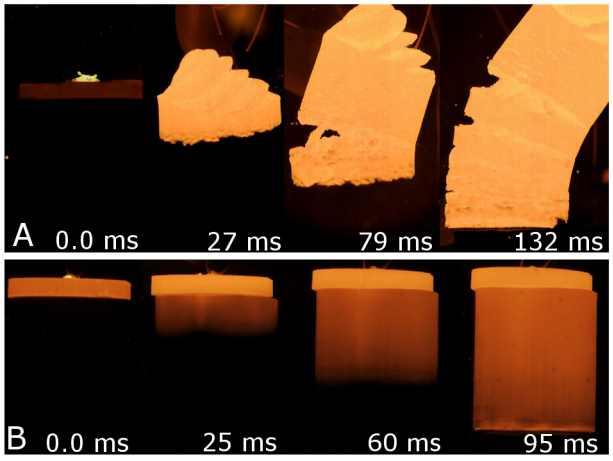


Figure 3.7. Still images from a typical combustion experiment for a pellet of Ni/Al material milled for A) 25% $t_{cr}$ and B) 75% $t_{cr}$.

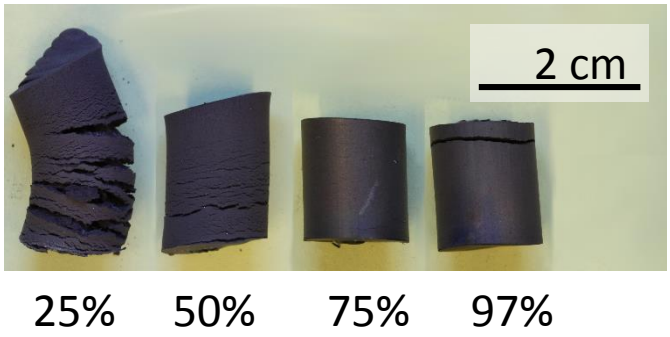


Figure 3.8. Visual comparison of the product NiAl pellets as a function of dry milling time (% $t_{cr}$).

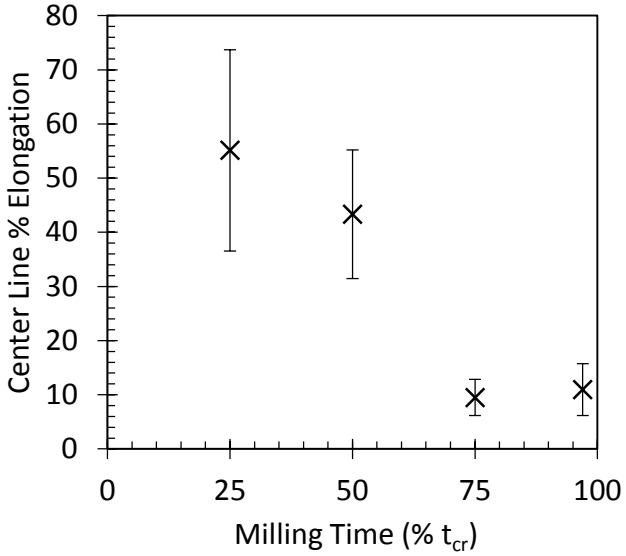


Figure 3.9. Center line % elongation of product NiAl pellets.

### 3.3.4 Microscopic Combustion Observation

To better understand why the expansion varies with milling time additional combustion experiments were preformed that consisted of combustion tests using a microscopic lens with a resolution of 8 $\mu m/pixel$ attached to the high speed camera, so that a close up image of the reaction front could be seen. In all of the samples tested gas formation was evident with the observation of particle ejection from the surface of

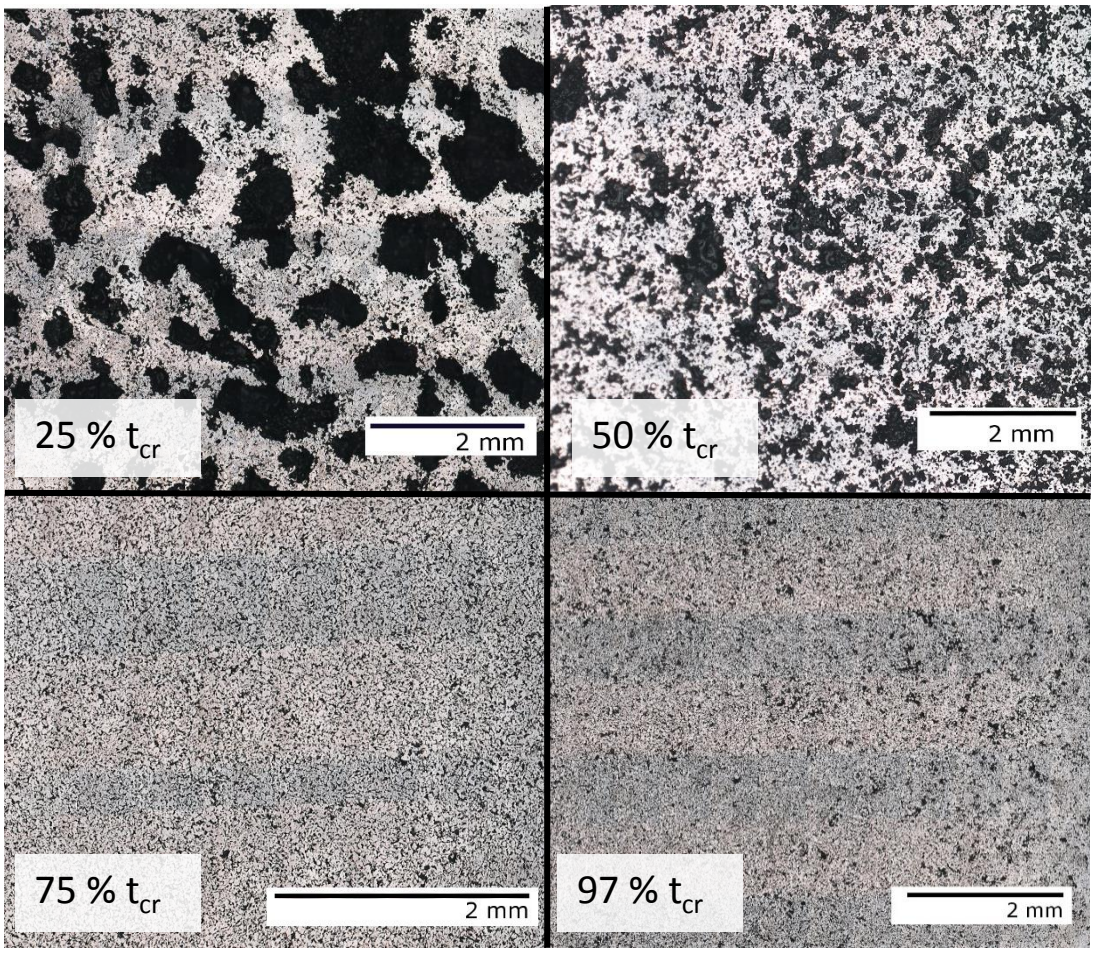


Figure 3.10. Optical microscope images of cross sectioned product pellets for dry milling time (% $t_{cr}$).

the pellet at the reaction front. However, for pellets with material milled for 25% $t_{cr}$ gas bubbles immediately formed on the pellet surface just behind the reaction front (see Figure 3.11 a and b). After about 10 $ms$ the bubbles collapsed. In figure 3.11 a) and b) the non-reacted MA Ni/Al can be seen above the black dashed line and is gray in color. After the front passes the material emits orange light, corresponding to its combustion temperature. For pellets with material milled for 97% $t_{cr}$ no gas bubbles were formed and individual particles clearly retained their shape. The observed bubbling indicates that there is a significant amount of degassing from within the pellet. It can be expected that the degassing is due to hydrocarbon contamina-

tion and entrapped air in the pressed pellet that forms hot gases upon combustion, as other studies have shown significant contamination can occur when liquid process control agents are used in the milling process [40].

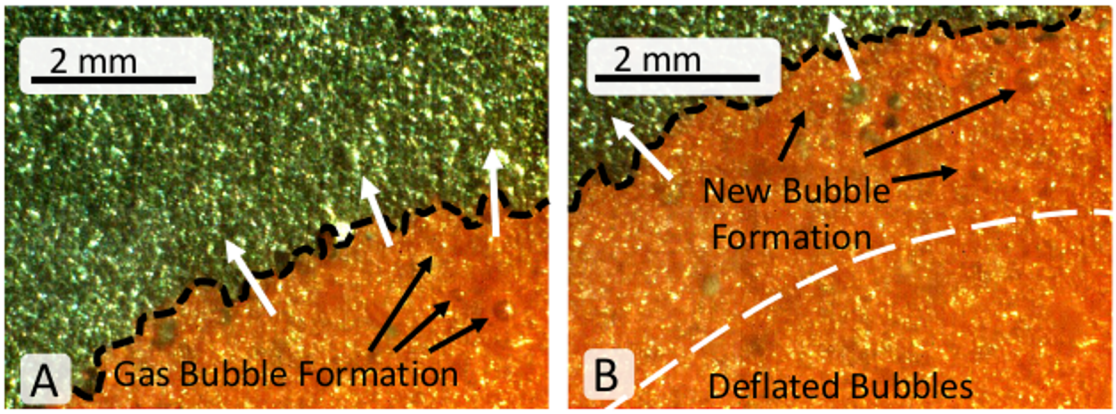


Figure 3.11. Close up images of the MA Ni/Al reaction front. Figures a) and b) are two frames from the combustion event of a pellet with material milled for 25% $t_{cr}$. The dashed black lines indicate the combustion front, the white arrows indicate the direction of reaction front propagation, and the dashed white line indicates the area after the front where bubbling ceases.

### 3.3.5 Thermal Analysis and Gas Phase Product Characterization

The presence of these contaminants and their release during reaction was confirmed by DSC/TGA coupled with FTIR. Integration of the total IR absorption spectra (Figure 3.12) shows that during DSC/TGA heating, the gas release begins at the onset of the second exotherm and continues throughout the reaction and corresponds to a simultaneous weight loss (see Figure 3.13). The FTIR spectra from evolved gas during the second exothermic reaction (Figure 3.14) indicate evolution of n-Hexane, ethane (from hexane decomposition), carbon dioxide, and water.

The evolution of hexane and ethane at temperatures ranging from 500-775 $K$, well excess of their boiling temperature, suggests the source is hydrocarbon contamination

within the particles by trapped porosity or chemical adsorption). The contaminates are likely released with the formation of cavities during the second exotherm [4]. Previously published SEM images of these materials [4] clearly show that cavities are formed between the laminate layers in the composite particles during the second exotherm and not before (see Figure 3.15). The formation of the cavities is likely due to extreme pressures from within the particle caused by the gasification of heating of chemically adsorbed or porosity trapped hexane. Recent work has shown that chemical adsorption may be expected when liquid hydrocarbons used in the milling of metals [40, 41]. Another factor that may possibly contribute to the formation of cavities are the differences in density, thermal expansion coefficients, and brittleness between the Al, Ni, and intermediates that from during the second exothermic reaction ($Ni_2Al_3$ and $NiAl_3$) [42].

The degree of contamination, as measured by TGA weight loss, decreased with increased milling duration. The weight loss ranged from $0.037 \pm 0.001\%$ for material milled to 25% $t_{cr}$ to about $\sim 0.013 \pm 0.003\%$ for material milled to 97% $t_{cr}$ (Figure 3.16). The larger concentration of hydrocarbon contamination observed in the material milled for dry milling times of 25 and 50% $t_{cr}$ may be due to greater material ductility at the start of the wet milling process as compared to the material with dry milling times of 75 and 97% $t_{cr}$. Greater material ductility during wet milling would cause increased cold working on the material, leading to higher concentration of hydrocarbon contamination

The slight amount hydrocarbon contamination in these materials will result in significant gas production upon reaction of the MA Ni/Al. Assuming the wt. loss is due to pure hexane, the volumetric equivalent for gaseous hexane at room temperature would range from 0.37 to 1.07 $mL/g$ of MA Ni/Al (see Table 3.1). Volumetric gas production at the maximum combustion temperatures measured in the combustion experiments was predicted by thermochemical equilibrium calculations using the equilibrium code Cheetah 5.0. Assuming that the hydrocarbon contamination is pure hexanes and taking into account the available air within the porous compact cal-

culations predicted volumetric gas releases of 2.34-5.95 $mL/g$ of MA Ni/Al, which is 12-30x the volume of the unreacted Ni/Al material (0.193 $ml/g$). These calculations clearly show that slight amounts of hydrocarbon contamination can result in significant gas production during combustion of the Ni/Al material.

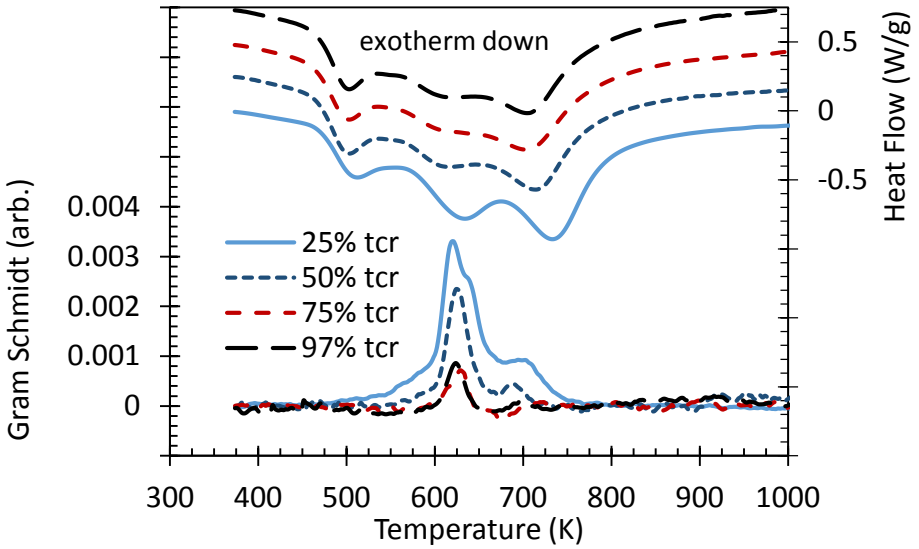


Figure 3.12. Gram Schmidt integrated intensity and heat release from DSC/TGA-FTIR measurements. Heat flow data is offset by ~0.2 $W/g$ for presentation.

Table 3.1. Equivalent gas volume production due to hydrocarbon contamination for 1 $g$ of MA Ni/AL.

| Milling Time (% $t_{cr}$) | Wt. of Hexane ($g$) | Pure Gaseous Hexane at 300$K$ ($mL$) | Predicted Gas Production at Max Temperature ($mL$) |
|---|---|---|---|
| 25 | 0.00038 | 1.07 | 5.95 |
| 50 | 0.00035 | 0.98 | 5.49 |
| 75 | 0.00015 | 0.44 | 2.68 |
| 97 | 0.00013 | 0.37 | 2.34 |

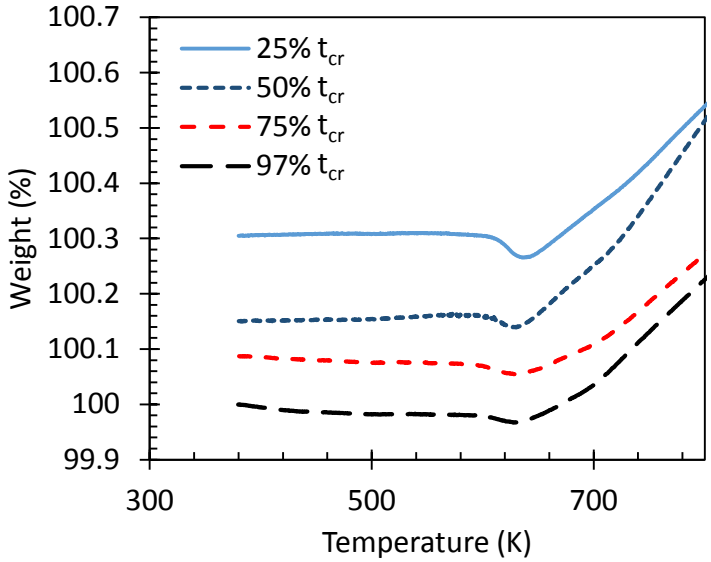


Figure 3.13. Thermogravimetric weight acquired from DSC/TGA measurements. Weight data is offset by ∼0.05-0.2% for presentation.

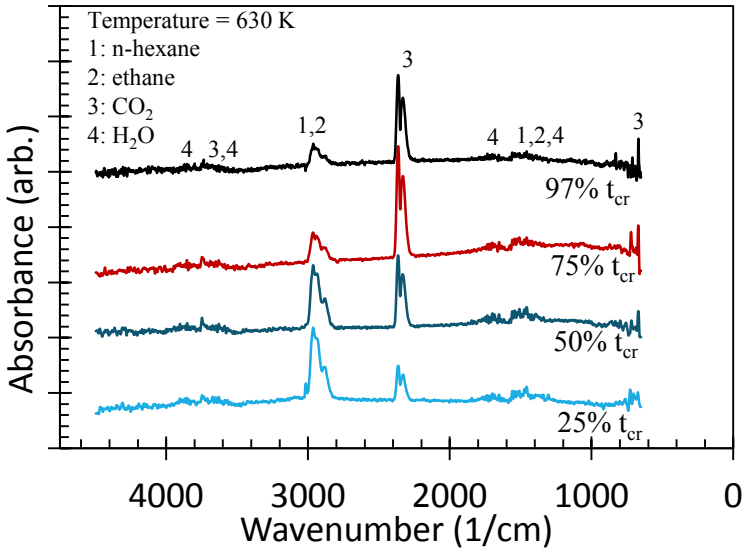


Figure 3.14. Infrared spectra collected at a temperature of 630 $K$ during DSC/TGA heating of MA Ni/Al.

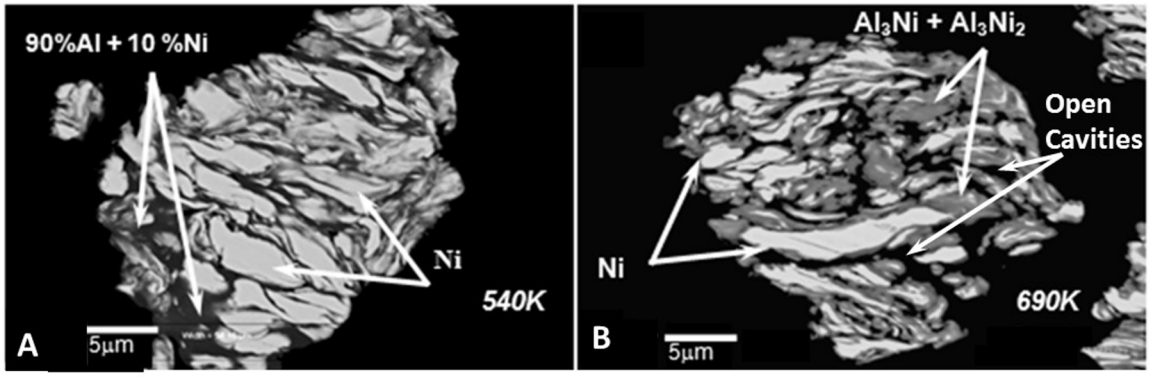


Figure 3.15. Scanning electron micrographs of 25% $t_{cr}$ particles after annealing at temperatures of 540 $K$ (A) and at 690 $K$ (B) [4]. Adapted with permission from Manukyan *et al. Journal of Physical Chemistry C* 2012, 116, 21027, http://dx.doi.org/10.1021/jp303407e. Copyright 2012 American Chemical Society.

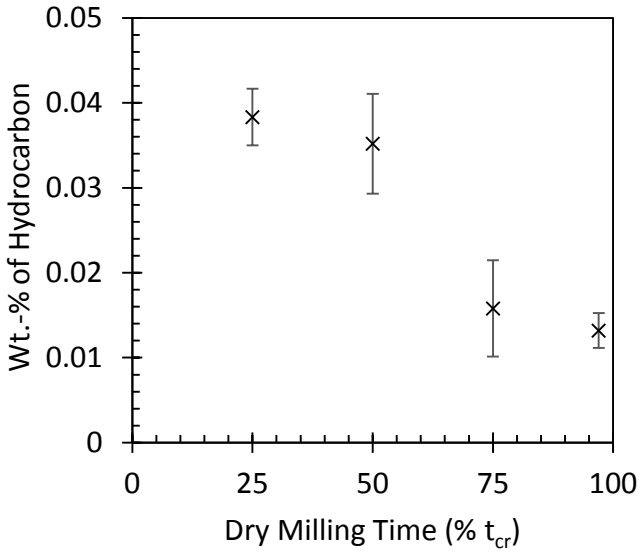


Figure 3.16. Percent wt. loss due to hydrocarbon contamination acquired from TGA measurements.

### 3.4 Conclusions

This work shows that modifying duration of dry milling significantly influences the combustion behavior of MA Ni/Al. Increasing dry milling duration can more than double the combustion velocity with a ∼5% reduction in flame temperature likely cased by the formation of amorphous or solid solution phases during.. This indicates that For MA Ni/Al pellets pressed to 70% TMD, the combustion velocities increase as the milling time increases from ∼9.4 $cm/s$ at a milling time of 25% $t_{cr}$ to ∼20 $cm/s$ at a milling time of 97% $t_{cr}$. Maximum combustion temperatures were measured to decrease as a function of milling duration from near adiabatic temperatures in the range of 1873 ± 30 $K$ for samples milled at 25 % $t_{cr}$ to an average about 1786 ± 30 $K$ for material milled at 97% $t_{cr}$. Extended dry milling was also found to reduce expansion during combustion and led to near net shape combustion products. In pellets consisting of material milled for 50% $t_{cr}$ or less the outgassing the formation of large pores due hydrocarbon contamiantion resulted expansion of up to 75% of the original length during combustion. For pellets consisting of MA Ni/Al material milled for 75% $t_{cr}$ or greater, the expansion due to outgassing was about 10%. Results from DSC/TGA coupled with FTIR confirms the hydrocarbon evolution at ∼630 $K$ which coincides with the formation of $Ni_2Al_3$ and $NiAl_3$. The DSC/TGA results also show that the concentration of hydrocarbon contaminants decrease with longer dry milling times, suggesting that the degree of contamination is affected by strain hardening during the dry milling treatment. Estimates of the degree of contamination are less than about 0.045 wt.-% in all cases and correspond to a gas evolution of about 2-6 $mL/g$ of MA Ni/Al powder. This indicates even low levels of contamination can significantly affect expansion of the product pellet, but that pellet expansion and final porosity can be controlled by dry milling time. This understanding has potential to greatly improve the quality (e.g. porosity) of all near net shape combustion synthesized materials. The limited expansion observed in these materials at milling times above 75% $t_{cr}$ could make these materials ideal for

applications such as cold-spray coating where little to no expansion upon combustion is desired. In addition, this demonstrates that stable liquid inclusions can be formed inside milled reactives, which could be considered as a way to modify reactivity.

# 4. EFFECT OF ANNEALING ON THE THERMAL RESPONSE AND DELFLAGRATION BEHAVIOR OF MECHANICALLY ACTIVATED NI/AL COMPOSITE POWDER

## 4.1 Introduction

In equiatomic MA Ni/Al mixtures, MA has been shown to decrease thermal ignition temperatures by up to 400 $K$, from the eutectic point ($\sim$912 $K$) to as low as $\sim$500 $K$ [4]. Thermal analysis using differential scanning calorimetry has revealed at least three exothermic peaks and it has been shown that the increase in thermal and impact ignition sensitivity is largely dictated by the first observed exothermic reaction [4,18]. X-ray diffraction of samples that have been annealed up to or just beyond the peak of the first exotherm have shown that the kinetics of the first exothermic reaction is due to the initial dissolution of Ni into Al [4, 19], and the formation of $NiAl_3$ [4, 19, 43]. Others have indicated that the first exothermic peak also consists of the release of stored mechanical energy acquired during milling [34, 35]. It has been shown that the onset of this first exothermic reaction decreases as the milling duration increases, and reaches a minimum when thinning of the Ni/AL structures/laminates during milling produces predominantly nanolaminate structures [18]. Further characterization of the mechanisms of the first reaction and their role in combustion would be useful in fundamentally understanding this material and could allow better tailoring of reactive materials. Recent studies have suggested that this decrease in activation energy is primarily due to stored energy and large defect densities due to plastic deformations [30, 34], but others have indicated that the stored energy due to plastic deformation is not sufficient to explain the such large decreases in ignition temperatures and accredited the decreases to mixing on the nano-scale mixing, increases in interfacial area per volume and the formation of amorphous/non-equilibrium phase

boundaries with no oxide layer. [23, 44]. Similar to past studies that have determined that the formation of the first exothermic reaction is due to the initial dissolution of Ni into Al [4, 19], and the formation of $NiAl_3$ [4, 19, 43], annealing these materials at different levels and characterizing the resulting materials could be used to further clarify the mechanisms that are responsible for the first exothermic peak, and what their effect on the resulting combustion velocities and temperatures are, specifically the effects of stored mechanical energy, and energy from initial intermetallic formation. In this work the objective is to more clearly determine the mechanisms and role of the initial exothermic reaction(s) on the thermal characteristics and overall combustion kinetics of MA Ni/Al. For this purpose, MA composite powders were annealed at different temperatures and X-ray diffraction (XRD) was used to determine the phase formation, amount of strain relaxation and grain growth. Differential scanning calorimetry (DSC) was used to measure the amount of heat released and to calculate adiabatic reaction temperatures. Green cylindrical compacts were pressed using the powders and ignited to measure reaction front velocities and temperatures as a function of annealing.

## 4.2 Experimental

### 4.2.1 Material preparation

For this work the mechanical activation procedure used was the same as in the previous chapters (see section 2.2.1) except that only material milled at 75% $t_{cr}$ was used. The material used for the work in this chapter was also sieved powder in the particle size range of 25-53 $\mu m$.

Annealing on the sieved MA Ni/Al powder was performed in a tube furnace under constant flow (300 $ml/min$) of ultra-high purity Ar (99.999%). The annealing temperatures were selected from DSC scans of as-milled material. The first temperature (403 $K$) was before of the first sharp exotherm and was chosen so that strain would possibly be released from the milled material without significantly affecting the heat

release of the first sharp exotherm. The second temperature (460 $K$) was at the onset of the first sharp exotherm and was chosen to initiate and complete the reactions of the first sharp exotherm without affecting the kinetics of the 2nd and 3rd exotherms. The samples were heated up to the target temperatures at a rate of 5 $deg/min$ and then held at that temperature for 30 $min$. afterward, the furnace was turned off and the material was cooled under the constant flow of Ar.

### 4.2.2 Microstructural Characterization

The microstructure of as-milled and annealed materials were examined by scanning electron microscopy (SEM) with a FEI-Magellan 400 field-emission scanning electron microscope (FESEM). The XRD analysis was performed using a Brunker D8 Focus with a LYNXEYE detector operated at a scanning speed of 1 $deg/min$ for the angular range of 30100° ($2\theta$) and a step size of 0.02°.

### 4.2.3 Thermal Analysis

Thermal properties were measured in a TA Instruments Q600 simultaneous thermogravimetric analyzer and differential scanning calorimeter (TGA/DSC). In each scan, $\sim$20 $mg$ of reactive material was heated to 1073 $K$ at a heating rate of 10 $K/min$ in an atmosphere of 99.999% pure Ar with a flow rate of 100 $cc/min$. For each condition, the sample was thermally cycled twice; the first time to measure the heat release and the second time to acquire a heat release baseline. The overall heat release of the reaction was measured after the heat release baseline was subtracted from the initial heat release measurement.

### 4.2.4 Combustion Experiments

Cylindrical pellets pressed to 70 ± 2% TMD with a height 13.5 ± 0.2 $mm$ and a diameter of 12.7 $mm$ were thermally ignited to acquire burning rates and combustion temperatures. The same procedure as outlined in section 3.2.2 was used.

## 4.3 Results and Discussion

### 4.3.1 Microstructure

The SEM images of typical particle cross sections show that the overall morphology was similar for each sample with the typical folded laminates with varying submicron dimensions. High magnification images (Figure 4.1) show very little difference in the Ni/Al laminate microstructure, except that in the case of the annealed material at 460 $K$, $NiAl_3$ nucleation sites are visible (Figure 4.2), similar to the growth of $NiAl_3$ in Ni/AL multilayer foils [45]. The $NiAl_3$ started forming at the interfaces at multiple nucleation sites and grew hemispherically as Ni diffused into the Al rich regions.

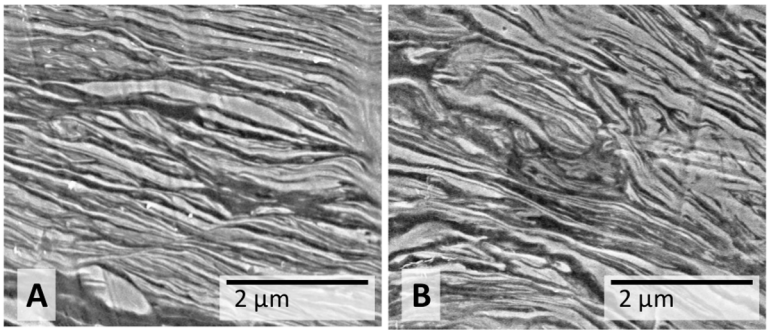


Figure 4.1. Typical laminate microstructures for A, non-annealed material and B, annealed at 460 $K$ at a magnification of 50,000x. The light areas are Ni and the dark areas are Al.

X-ray diffraction was performed to identify crystallite size, strain, and phases formed for each powder. Figure 4.3 shows the peak profiles obtained for the 3 ma-

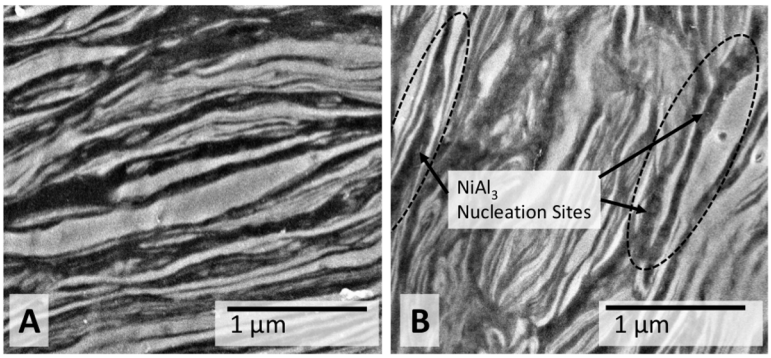


Figure 4.2. Typical laminate microstructures for A, non-annealed material and B, annealed at 460 $K$ at a magnification of 100,000x. The light areas are Ni and the dark areas are Al.

terials. In as-milled and 403 $K$ annealed material, only Ni and Al peaks could be detected. For 460 $K$ sample, the $NiAl_3$ peaks were clearly visible, confirming the formation of $NiAl_3$ during the higher temperature annealing procedure. The strains and grain sizes were determined using Williamson-Hall analysis on the well-resolved non-overlapping peaks for qualitative comparison between samples (Figure 4.4). The crystal planes used were (111) and (311) for Al, and (200), (220) and (311) for Ni. Table 4.1 and 4.2 shows the resulting crystallite size and strain calculated. The as-milled sample had an average percent strain of 0.34 for Ni and 0.39 for Al indicating that both materials are deformed and strained in comparable amounts, as also seen in the SEM images. The average grain sizes are 36 $nm$ for Ni and 58 $nm$ for Al. After the 403 $K$ annealing, the strains were relieved to 0.22 and 0.29 and the grain sizes were reduced slightly to 28 and 48 $nm$ for Ni and Al respectively. Although this is within the error in the measurements, it is plausible that some recrystallization might have occurred at this stage. For the 460 $K$ annealing, in addition to reduced strains of 0.26 and 0.24 which are comparable to the 403 $K$ annealed sample, significant grain growth was observed for Al with average grain sizes around 110 $nm$, whereas Ni grains remained small around 35 $nm$.

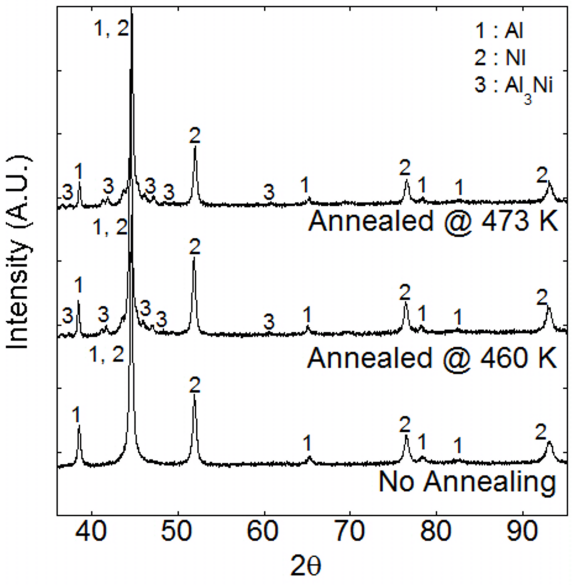


Figure 4.3. X-Ray diffraction traces as a function of annealing.

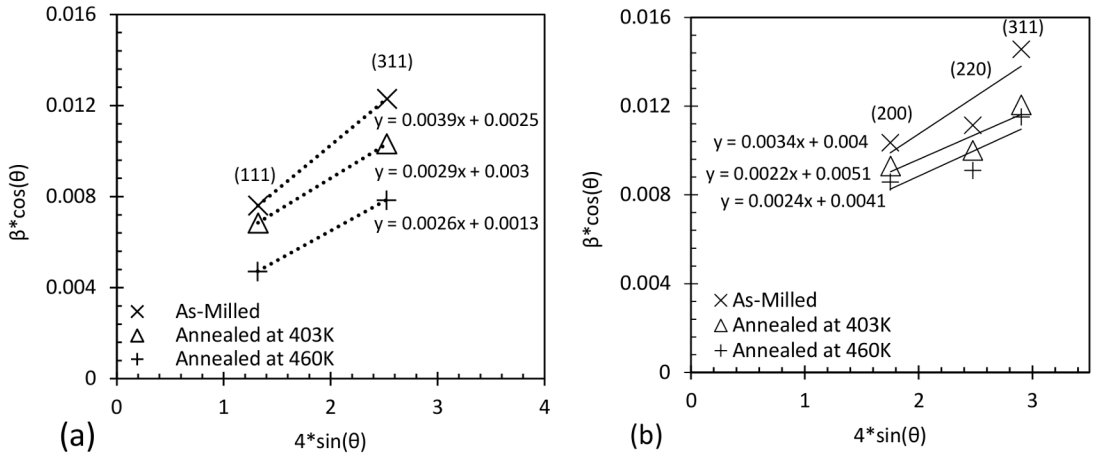


Figure 4.4. Williamson-Hall plot for (a) Al and (b) Ni peaks measured from the MA Ni/Al reactive mixture powders as a function of annealing.

### 4.3.2 Thermal Analysis

DSC measurements were performed on the three materials to identify how the different annealing conditions affect the kinetics and heat release of the MA Ni/Al

Table 4.1. Strain and Crystallite size acquired from Williamson-Hall plot for Ni peaks measured from the MA Ni/Al reactive mixture powders as a function of ball milling time.

| Material | Slope/Strain | Size ($nm$) |
|---|---|---|
| As-Milled | 0.0034 | 36 |
| Annealed at 403 $K$ | 0.0022 | 28 |
| Annealed at 460 $K$ | 0.0024 | 35 |

Table 4.2. Strain and Crystallite size acquired from Williamson-Hall plot for Al peaks measured from the MA Ni/Al reactive mixture powders as a function of ball milling time.

| Material | Slope/Strain | Size ($nm$) |
|---|---|---|
| As-Milled | 0.0039 | 58 |
| Annealed at 403 $K$ | 0.0029 | 48 |
| Annealed at 460 $K$ | 0.0026 | 111 |

composites (Figure 4.5). As-milled material behaved as previously reported [4, 18], where an initial low exotherm starting around 403 $K$ is followed by 3 larger exothermic peaks. The 403 $K$ annealed material had a very similar DSC curve, but it was missing the initial low exotherm and just showed the 3 sharp peaks. Indicating that there is a slight energy loss associated with strain relaxation. For the material annealed at 460 $K$ the low exotherm not observed and the first sharp peak was almost completely missing, while the 2nd and 3rd peaks were identical to the other samples. The measured overall heat release values and the corresponding adiabatic temperatures are given in Table 4.3. The adiabatic temperatures were calculated using a similar approach to Zhu *et. al* [46] with enthalpy offsets to account for the reduction in reaction heat and assuming complete conversion into the NiAl phase. The calculated temperature for the 460 $K$ annealed sample was 1688 $K$ and significantly lower than the other samples, which were 1874 $K$ and 1852 $K$ for the as-milled and 403 $K$ annealed samples respectively.

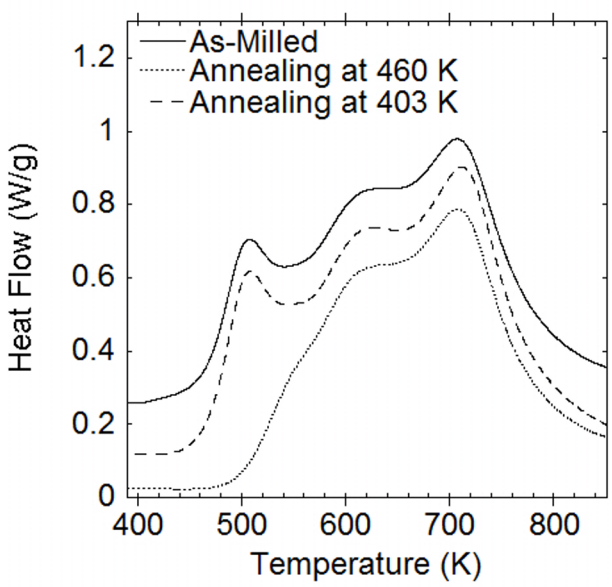


Figure 4.5. DSC/TGA Traces for MA Ni/Al reactive mixture powders as a function of annealing temperature.

Table 4.3. Reaction onset temperatures, heat of reactions, and calculated adiabatic temperatures.

| Material | Initial On-set Temperature ($K$) | Exothermic Heat Release ($J/g$) | Calculated Adiabatic Temperature ($K$) |
|---|---|---|---|
| As-Milled | 462 | 1050 | 1874 |
| Annealed at 403 $K$ | 465 | 1033 | 1852 |
| Annealed at 460 $K$ | 500 | 906 | 1688 |

### 4.3.3 Combustion Experiments

The combustion velocities are shown in Figures 4.6 . The pellets consisting of as-milled material and material annealed at 403 $K$ had average combustion velocities of $\sim$16 $cm/s$, whereas the material annealed at 460 $K$ had average combustion velocities of 5 $cm/s$. The low temperature annealing (403 $K$) did not affect the velocity, so the strain recovery had minimal effect on the reaction kinetics. 4.7 shows the maximum combustion temperatures measured by IR using an emissivity of 0.925. For these samples the emissivity was found to be in the range of 0.90-0.95 when fitting the IR

measurements to the maximum temperature and initial cooling of the temperature profile of the thermocouple. The thermocouple could not capture the initial rapid rise due to thermal lag, therefore the FLIR temperatures measured during and just after the initial temperature rise have some uncertainty as the formation of intermetallics and oxidation will likely affect the emissivity the material. The temperature profiles as a function of time for the samples are shown in Figure 4.8. These temperatures, measured using IR and an emissivity of 0.925, showed a rapid rise as the front moved across the measurement point and then continued to rise for another ∼600-1500 $ms$. In the case of pellets as-milled and annealed at 403 $K$ the measurements show a rapid rise to 1700 ± 50 $K$ and then reached the maximum temperature of about 1835 ± 40 $K$ in about ∼600-900 $ms$. For the pellets with material milled to 460 $K$ the temperature rose rapidly to 1615 ± 65 $K$ and then gradually increased to the maximum temperature of 1700 ± 40 $K$ in ∼1200-1700 $ms$. The maximum temperature values were comparable to the adiabatic temperatures calculated from the DSC analysis. The initial rapid reaction stage is due to the rapid growth formation and growth of intermetallics such as $NiAl_3$, $Ni_2Al_3$, and then NiAl. The gradual increase in temperature may be due to continued but slower formation of intermetallic product and/or oxidation of the product. In the case of the material annealed at 460 $K$ the initial rapid temperature raise is also slightly slower than the other two cases indicating that the reaction kinetics are occurring at a slower rate than for the as-milled and annealed at 403 $K$ materials, which is expected as the combustion velocity is 10 $cm/s$ slower.

Since for all the samples, the particle size and morphology are similar, the large variation in combustion velocities observed for material annealed at 460 $K$, are likely attributed to the lower combustion temperatures, changes in activation energy, and differences in interface kinetics within particles such as the pre-formation of the $NiAl_3$ phase during the annealing. As indicated by the DSC and XRD results, the lower combustion temperatures are mainly due to the decrease in energy output caused the formation of the $NiAl_3$ phase during annealing. The lower temperatures along with an

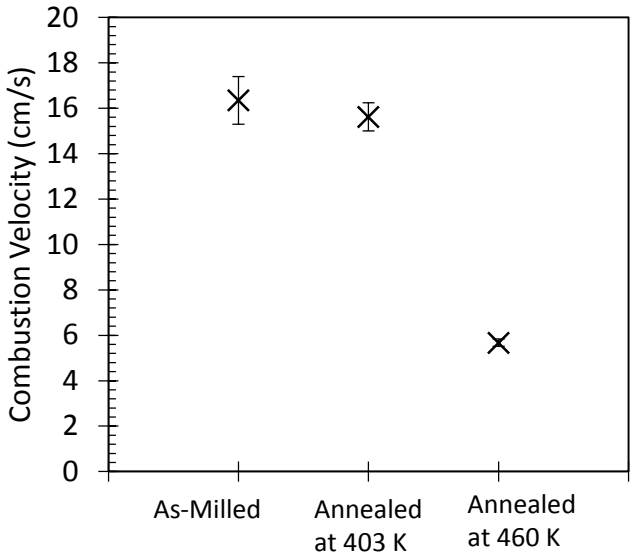


Figure 4.6. Combustion velocities of Ni/Al compacts (Error bars indicate the standard deviation of the experiments).

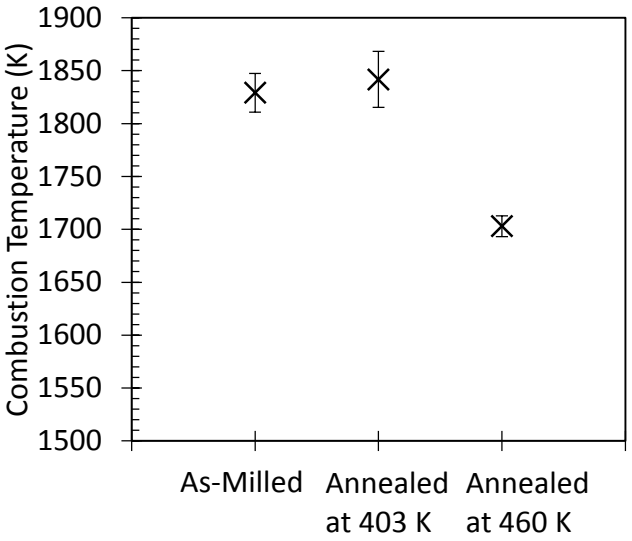


Figure 4.7. Average maximum combustion temperatures of MA Ni/Al compacts as measured by FLIR with assuming an emissivity of 0.925. (Error bars indicate one standard deviation and the uncertainty due to emissivity is $\pm$ 30 $K$.

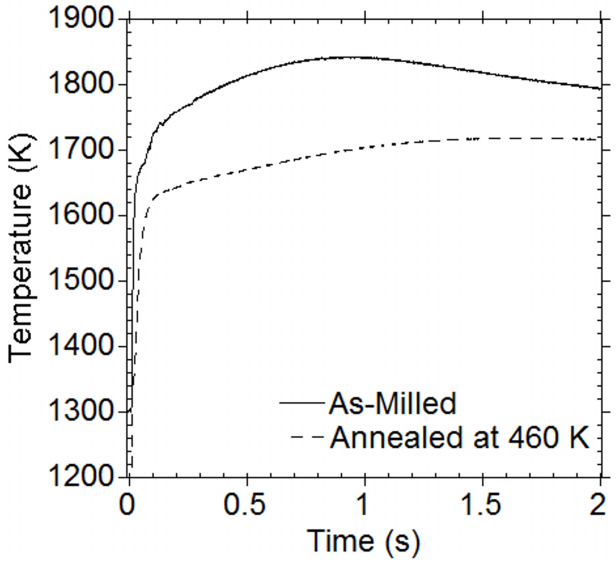


Figure 4.8. Typical combustion temperature profiles measured by IR camera assuming an emissivity of 0.925.

expected decrease in activation energy due to the higher onset temperature observed in DSC results would result in slower reaction rates within each particle and delay the ignition of neighboring particles, yielding slower combustion front velocities [44]. Such behavior can be expected to reduce sensitivity as well, which also depends on the initial reaction kinetics.

## 4.4 Conclusions

The work in this chapter shows that the initial intermetallic formation of $NiAl_3$ formed by annealing at the initial thermal onset temperature has a significant effect on the combustion velocities and temperatures MA Ni/Al green compacts, while the relaxation of strain only, did not. To understand this effect, Ni/Al powders were mechanically activated using high energy ball milling and then annealed at 403 or 460 $K$. The particles were characterized using electron imaging, x-ray diffraction and differential scanning calorimetry (DSC). Combustion experiments were performed to measure the reaction velocities and temperatures using high-speed infrared imaging

and thermocouples. Williamson-Hall analysis suggests that recovery occurs at an annealing temperature of 403 $K$ resulting in lower strains for both Al and Ni. At an annealing temperature of 460 $K$, both recovery and Al grain growth was observed along with the growth of $NiAl_3$ phase, which was also detected using scanning electron microscopy. The morphology and characteristic laminate dimensions were not significantly affected by annealing. The annealing at 403 $K$ had little effect on combustion velocities and temperatures and were measured to be $\sim$16 $cm/s$ and $\sim$1835 $\pm$ 40 $K$ respectively. The annealing at 460 $K$ significantly reduced combustion velocities and temperatures down to $\sim$6 $cm/s$ and 1700 $\pm$ 30 $K$ respectively. The temperatures were slightly under adiabatic temperatures calculated from heat of reactions measured from DSC analysis. The results show that the front velocities and maximum temperatures are largely influenced by the formation of $NiAl_3$ during annealing at 460 $K$, which is also expected to reduce particle ignition sensitivity.

# 5. THE EFFECT OF MILLING JAR AND MEDIA SURFACE CONDITION ON THE MECHANICAL ACTIVATION OF NI/AL

## 5.1 Introduction

Processing control agents (PCA) are routinely used in milling metal powders in order to reduce particle sizes and increase material yield. The PCA accomplishes both of these objectives by preventing cold welding of the milled particles to each other and to the milling jar and media [40]. If no PCA is used, the resulting yield could be low if most the material is cold welded to the jar walls and balls, or the resulting particle sizes could be much larger than the initial material particle sizes if the particles are cold welded to each other during the milling [40, 47]. The use of a PCA can significantly reduce both of these effects, however, with significant drawbacks. With the use of PCA, significant carbon, oxygen, and hydrogen contamination can occur [40]. This contamination can be chemically adsorbed, and can form carbides, hydrides, and oxides that can increase hardness, leading to poor structural integrity when pressed [40, 48–51]. PCA can also inhibit the formation of lamellar microstructure [52, 53], which in turn may require longer milling times in order to reach the same level of microstructural refinement compared to a case if no PCA was used. In order to reduce contamination but still obtain usable material after milling, two-step milling methods that consist of a dry milling step followed by a wet (PCA) step have been used [22, 54, 55]. During the dry milling stage, a large amount of the initial materials are cold welded to the milling jar, media and each other, resulting in large milled particles. The wet milling step then breaks up the cold welded material thereby reducing particle sizes and increasing the usable material yield [4, 22, 55]. Recently, two-step wet/dry milling procedures have been used to produce MA reactive composite powders of Ni/Al in order to maximize microstructure refinement and particle

size reduction [4, 22, 55]. During the dry milling stage, the initial materials are cold welded to the milling jar, media and each other, resulting in large Ni/Al composite particles and a large amount of material cold welded to milling jar and balls. The material is then wet milled in hexane to reduce the particle size [4, 22, 55]. It is not fully understood what role that cold-weld material plays in regards the final yield of the material, its milled microstructure and if it affects the combustion performance of the resulting material. In theory the amount of material cold-welded to the milling jar and media may possibly vary if the milling jar and ball surfaces are treated with a PCA. This could possibly be done when the jar is cleaned between milling runs. On this regard, objective of the work in this chapter is to determine if the amount of cold welding during the dry milling stage can be varied if hexane rather than water used to clean the milling jar in-between milling runs, and if it can, how does varying the amount of cold welding in the mechanical activation process affects the resulting mixture yield and the combustion behavior of MA Ni/Al powders.

## 5.2 Experimental

### 5.2.1 Material preparation

The material used in the chapter was prepared same manner as described in previous chapters with some variation. Aluminum (Alfa Aesar, particle size -325 mesh, lot. K27Y032) and nickel (Alfa Aesar, particle size 3-7 $\mu m$, lot. E26X037 and E22Z013) powders were milled using at of an equiatomic Ni+Al mixture. The material was milled using a two-step milling procedure as previous descried. In all cases the material was first dry milled for a total 12.75 $min$ or 75% $t_{cr}$ and the wet milled in 20 $mL$ of hexanes at $\sim$0.3 MPa. In all cases the material was milled in a high purity (99.998%) argon atmosphere. After wet milling the samples were dried in air for 1 $hr$ and then vacuum-dried at $\sim$300 $K$, for 24 $hr$ to remove any residue hexane. After the materials were dried for 24 $hr$, milling batch yields were measured by sieving the powder into six fractions, $<$25 $\mu m$, 25-53 $\mu m$, 53-106 $\mu m$, 106-355 $\mu m$,

355-850 $\mu m$, and >850 $\mu m$. The material having a particle size of 25-53 $\mu m$ was chose for further characterization in this study so that experiments are be comparable to the previous work.

Between each milling run, the milling jar and media was cleaned in order to remove cold-welded material remaining on the milling jar or media after the wet milling step. This cleaning was done using two different methods. The first method consisted of water cleaning and the second method consisted of hexane cleaning. The water cleaning consisted of performing a milling run with only the milling media and approximately 50 $ml$ of water. The milling run was performed at 550 rpm for 5 minutes. If residue cold welded Ni/Al material was visible after the water cleaning, the cleaning was then repeated until the jar appeared clean (typically 2-3 times). The hexane cleaning used the same steps except 20 $ml$ of hexane was used instead of water. In all cases, the jar and milling media were thoroughly rinsed and dried after the cleaning runs were performed.

### 5.2.2 Powder Characterization

The microstructures of the prepared MA Ni/Al materials were examined by scanning electron microscopy using a FEI-Magellan 400 field-emission scanning electron microscope (FESEM). Phase, strain and crystallite sizes were analyzed by X-ray diffraction (XRD) using a Brunker D8 Focus with a LYNXEYE detector operated at a scanning speed of 1 $deg/min$ for the angular range of 30-100° ($2\theta$) and a step size of 0.02°.

### 5.2.3 Thermal Analysis

Thermal properties were measured in a TA Instruments Q600 simultaneous thermogravimetric analyzer and differential scanning calorimeter (TGA/DSC). In each scan, $\sim$20 $mg$ of reactive material was heated to 1073 $K$ at a heating rate of 10 $K/min$ in an atmosphere of 99.999% pure Ar with a flow rate of 100 $cc/min$. For

each condition, the sample was thermally cycled twice; the first time to measure the heat release and the second time to acquire a heat release baseline. The overall heat release of the reaction was measured after the heat release baseline was subtracted from the initial heat release measurement.

### 5.2.4 Combustion Experiments

Cylindrical pellets pressed to 70% $\pm$ 2 % TMD with a height 13.5 $\pm$ 0.2 $mm$ and a diameter of 12.7 $mm$ were thermally ignited to acquire burning rates and combustion temperatures. The same experimental setup as outlined in section 3.2.2 was used.

## 5.3 Results and Discussion

### 5.3.1 Milling Results

As described in the experimental section above, the milling jar and media undergo a cleaning mill run between material milling runs with either water or hexane to remove any remaining cold welded material. Depending upon which solvent was used for the cleaning, the amount of Ni/Al material that was cold welded to the milling jar/media after the dry milling step of the next milling run varied. Figure 5.1 shows images of the milling jar with the milling media and the powder after the dry milling step using both cleaning methods. When water was used for the cleaning run, on average about 18 $g$ or $\sim$50% of the initial material would be cold welded to the milling jar and media during the actual milling with the remaining material in the form of Ni/Al composite particles having sizes in the range of 0.1  3 $mm$. When hexane was used for the cleaning run, on average about 10 $g$ or 30% of the initial material was cold welded. This difference in cold welding is due to the surface condition of the milling jar/media after cleaning. Additionally, when water was used during the cleaning milling run, the majority of residual cold welded Ni/Al material left on the milling jar from the previous run was removed from the walls and any

fresh metal surfaces are oxidized due to the presence of water. When hexane was used as the cleaning agent, the majority of residual cold welded Ni/Al material was also removed from the milling jars and media, but a barely visible thin coating Ni/Al remained and it is likely that hexane was covalently bonded to the surfaces, which is a typical result of using hexane as a PCA [40]. A thin coating layer of Ni/Al + hexane would reduce the amount cold welding between the Ni/Al and milling jar and balls [40]. After the material has undergone both dry and wet milling steps, there is a large difference in material yield between the two milling methods. Table 5.1 shows the typical yield as a function of sieved partial size range for each cleaning method. In both cases, particle sizes ranged from 3 $mm$ down to less than 25 $\mu m$. However, the yield of material less than 106 $\mu m$ is much higher if water is used for the cleaning rather than hexane ($\sim$12.5 $g$ vs. 4.5 $g$ respectively). This indicates that increased cold welding during the dry milling step will tend to result in an increase in particle refinement during the wet milling step. It is likely the case that during wet milling, the majority of the material that is refined into smaller particles originates from the material that is cold welded to the milling jar and media. An indicator of this is that weight of the material in the size range of 106-3000 $\mu m$ is typically about 4 $g$ more after wet milling than after dry milling for both cleaning methods, meaning that the majority of the larger particles are not likely being broken up during the wet milling process.

Table 5.1. Average material yield as a function of cleaning method ± one standard deviation.

| Size Range ($\mu m$) | Water Cleaned Jar Yield ($g$) | Hexane Cleaned Jar Yield ($g$) |
|---|---|---|
| <25 | 2.9 ± 0.5 | 2.5 ± 0.6 |
| 25-53 | 5.5 ± 0.6 | 1.4 ± 0.3 |
| 53-106 | 4.3 ± 0.3 | 0.8 ± 0.2 |
| 106-3000 | 17.4 ± 0.6 | 29.6 ± 1.1 |

Figure 5.2 shows typical cross-sectional SEM images of composite particles in the 25-53 $\mu m$ size range for material milled in the jar cleaned with water (material 1) and

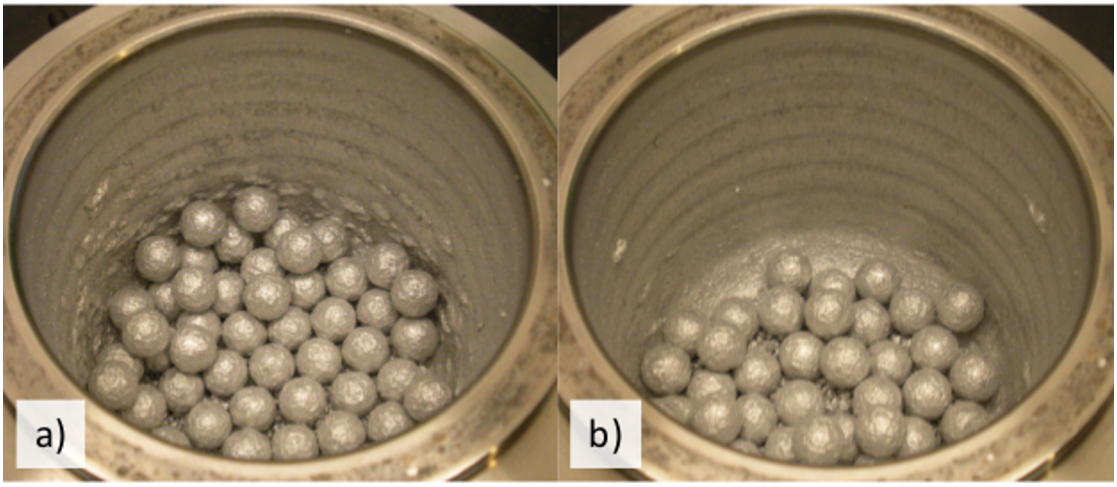


Figure 5.1. Images of the jar, milling media, and powder after dry milling for a) water cleaned jar and b) hexane cleaned jar. The same exposure and lighting was used for both cases.

hexane (material 2). The overall geometry was similar for each of the powders except that in the case of material 2, a large amount of voids and cracks were observed. It is possible that these particles have been fractured and re-welded multiple times. High magnification images (see Figure 5.2 c and d) show that each both materials have the typical nanolaminate features observed in MA material, but material 2 appears to have a higher degree of laminate folding.

X-ray diffraction was performed to identify crystallite size, strain and phases formed for each material. Figure 5.3 shows the peaks obtained for the two materials, where Al and Ni peaks are clearly visible. The full-width half maxima (FWHM) of Ni peaks were measured to be within 6% of each other, which is within sample to sample variation (<10%), indicating that the Ni in both samples have similar crystallite size and strain in the range of about 20-40 $nm$ and 0.25-0.35% respectively, which was calculated using Williamson-Hall analysis. Using just the (111) and (311) peaks ($2\theta \sim 38.5$ and 78), the Al in material 1 and 2 has a crystallite sizes of about 60 and 181 $nm$, respectively. The Al in both materials a strain of about 0.35-0.45%. The FWHM of Al peaks are similar with a variation of <7%, of except for the (220) and (222)

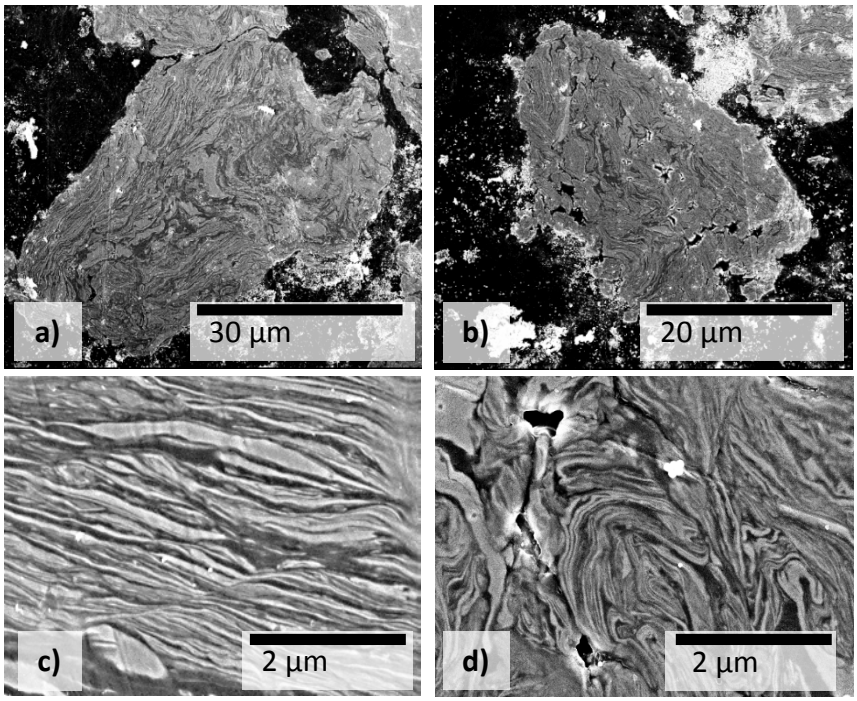


Figure 5.2. Typical laminate microstructures for a) material 1 and b) material 2 at 5,000x magnification and c) material 1 and d) material 2 at 50,000x magnification. The light areas are Ni and the dark areas are Al.

peaks ($2\theta \sim 65$ and 82). In material 2, these peaks are 50% and 85% broader than in material 1. NiAl and $Ni_2Al_3$ both have diffraction peaks at these peak locations. XRD at lower angles shown in Figure 5.4 provide direct evidence for the formation of NiAl and $Ni_2Al_3$ in material 2, with broad peaks at $2\theta \sim 26$ and 31. This also indicates that these phases consist of very fine nanocrystalline grains, comparable to Al and Ni.

### 5.3.2 Thermal Analysis

DSC measurements were performed in order to characterize the reaction kinetics for both materials. Material 1 behaved as previously reported [4, 18], exhibiting 3 exothermic peaks (Figure 5.5). Material 2, however, exhibits only 2 distinguishable

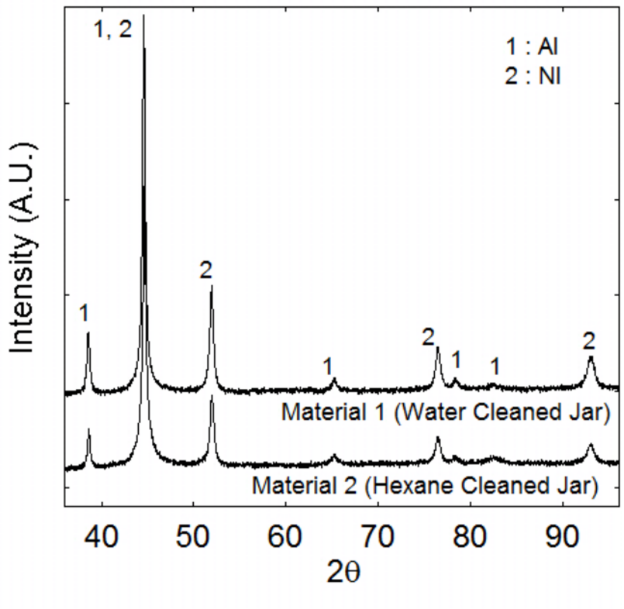


Figure 5.3. X-Ray diffraction measurements.

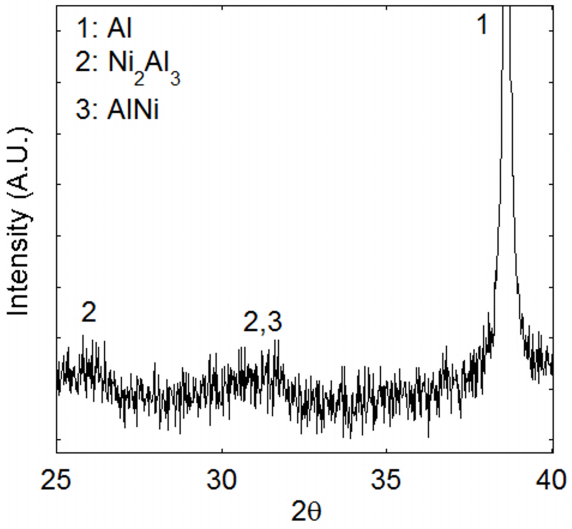


Figure 5.4. X-Ray diffraction measurements for material 2 showing broad $Ni_2Al_3$ peaks.

peaks, the first has the same onset temperature as material 1, but with slightly less heat release. The second peak is a combination of the second and third peaks except that the third peak is significantly reduced. It was previously reported that the second

peak correlates with the formation of $NiAl_3$ and $Ni_2Al_3$ and third with $Ni_2Al_3$ and NiAl [4]. The reduction in energy release can be attributed to the existence of $Ni_2Al_3$ and NiAl.

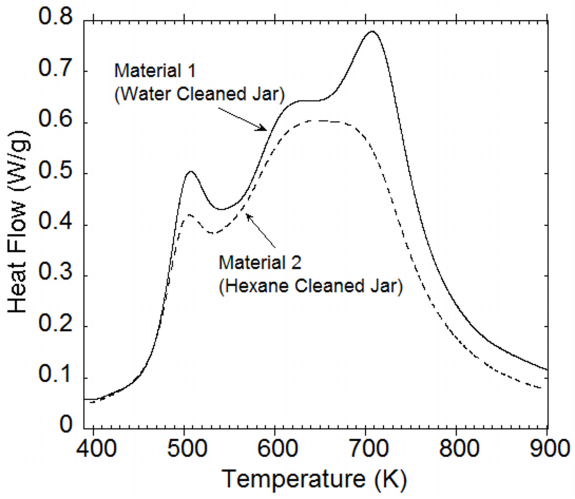


Figure 5.5. Heat release measured by DSC for each material.

### 5.3.3 Combustion Experiments

The combustion velocities and temperatures for the green compacts are shown in Table 5.2. Average combustion velocities were 16 ± 1.0 $cm/s$ and 10 ± 0.8 $cm/s$ for material 1 and 2 respectively. Temperature measurements were performed by IR imaging, where the emissivity was found by matching maximum temperature and cooling curves of the IR and thermocouple data (see Figure 5.6). The emissivity was 0.9-0.95 for material 1 and 0.97-1.0 for material 2. The thermocouple could not capture the initial rapid rise due to thermal lag. The temperatures measured using IR show a rapid rise as the front moved across the measurement point and then a more gradual rise for another ∼600-900 $ms$. Material 1 had an average maximum temperature of 1830 ± 30 $K$, while material 2 had an average maximum temperature of 1575 ± 17 $K$. The lower combustion temperatures and velocities in material 2 can

likely be attributed to the lower heat release as a result of the observed phases formed during milling.

Table 5.2. Combustion Velocities and Maximum Temperatures.

| Material | Combustion Velocity ($cm/s$) | Combustion Temperature ($K$) |
|---|---|---|
| 1 (Water Cleaned Jar) | 16 ± 1.0 | 1830 ± 30 |
| 2 (Hexane Cleaned Jar) | 9.8 ± 0.8 | 1575 ± 17 |

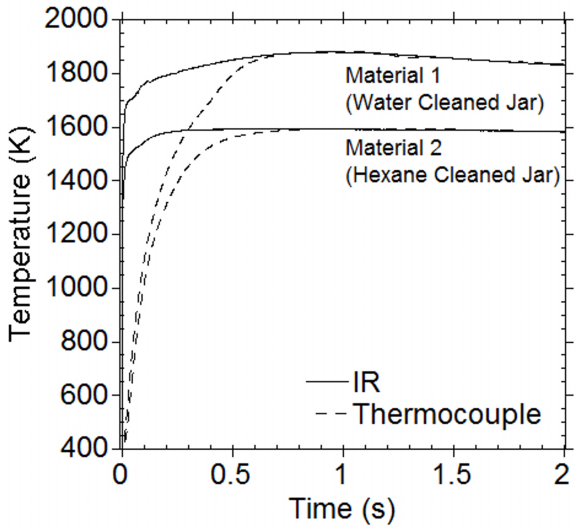


Figure 5.6. Typical combustion temperature profiles measured by IR camera and thermocouples.

## 5.4 Conclusions

This work shows that the initial surface condition of the milling jar and media for mechanical activation of metal-based reactives can have a large effect on the resulting material properties and combustion characteristics of the resulting MA material. When cleaning the milling jar between milling runs the cleaning agent can leave residues or leftover milled material on the surfaces, which affect the way milled material cold welds to the milling jar and media. In the case of hexane cleaning, the

surfaces of the milling jar and media had some hexane residue and possibly some small amount of Ni/Al following cleaning, which reduced the amount of cold welding in the subsequent dry milling runs. This reduced the final yield of fine particles (<106 $\mu m$) and resulted in the formation of intermetallics during milling, which lowered the overall heat output observed using DSC, compared to water cleaning. As a result of this heat loss, maximum temperatures and front velocities were also reduced in the combustion experiments. Water cleaning increased cold welding to the milling jar surfaces during milling and reduced the total amount of plastic work experienced by the particles, which retained most of their reactivity, resulting in higher combustion temperatures and velocities. The reaction onset temperatures in DSC were not affected by the cleaning agent.

# 6. CONCLUSIONS

The work in this dissertation shows that ignition sensitivity and combustion performance can be modified by refining the microstructure of MA Ni/Al reactive composite powder by adjusting the milling conditions, such as milling duration. It was shown that as the microstructure is refined by increased dry milling the impact and thermal ignition thresholds lower, combustion velocity increase and combustion temperatures and energy outputs decrease. As the dry milling time increases the impact ignition threshold decreases from an impact energy greater than 500 $J$ (200 $m/s$) for dry milling times of 25% $t_{cr}$ to ∼200 $J$ (130 $m/s$) at dry milling times of 50% $t_{cr}$. The impact ignition threshold then decreases to ∼40-60 $J$ (60-70 $m/s$) as the total dry milling time increases from 50% $t_{cr}$ to 97% $t_{cr}$. Ignition of the samples occurred at ignition spots typically on or near the impact face and edges of the sample. Ignition delays were found to be on the order of 1-6.5 $ms$ and combustion velocities were on the order of 20-31 $cm/s$. Increased milling had little effect on the ignition delays or combustion velocities of the impacted sample as long as the material was dry milled to at least 50% $t_{cr}$.

The impact ignition results along with DSC analysis indicate that i) the driving mechanism behind reaction upon impact for these experiments is the rapid increase in temperature at localized hot spots on or near the impact face and edges of the sample and that when the hotspots reach the thermal ignition threshold, the impacted sample ignites and ii) that although increasing milling time to near the critical milling time does continually reduce the thermal and impact thresholds, the reductions are modest beyond a point and may not be worth the potential loss in reaction energy due to extensive milling. Here we find that the largest jump in sensitivity is between the dry milling times of 25% $t_{cr}$ and 50% $t_{cr}$ corresponding to when nanolaminate structures are initially detected during the ball milling process. Thermal analysis

along with previous work indicates that the increase in the sensitivity to thermal and mechanical impact is dictated by a combination of three factors: the formation of microdeformations (vacancies and dislocations), amorphous Al, and nanolaminate structures, which reduce the temperature needed to begin the dissolution of nickel into aluminum. DSC analysis showed that between the dry milling times of 25% $t_{cr}$ and 50% $t_{cr}$ the onset of the dissolution of nickel into aluminum shifted from 479 $K$ to 462 $K$. Further dry milling of the MA Ni/Al does not reduce the onset of the dissolution of nickel into aluminum but it does reduce the total energy output of the system, indicating that for this system and method a milling time of about 50-75% $t_{cr}$ is likely optimal when taking into account both the increased ignition sensitivity of mechanical activation and potential loss in reaction energy with longer milling times.

Deflagration experiments for MA Ni/Al pressed green compacts into cylindrical pellets resulted in combustion velocities that increased as the milling duration increased from ∼9.4 $cm/s$ at a milling time of 25% $t_{cr}$ to ∼20 cm/s at a milling time of 97% $t_{cr}$. Maximum combustion temperatures were measured to decrease as a function of milling duration from 1873 ± 30 K for samples milled at 25% $t_{cr}$ to an average about 1786 ± 30 $K$ for material milled at 97% $t_{cr}$. It was also observed that during combustion the green compacts consisting of material milled for 50% $t_{cr}$ or less expanded by up to 75% upon combustion due the formation of large pores and outgassing. For pellets consisting of MA Ni/Al material milled for 75% $t_{cr}$ or greater, the expansion due to outgassing was about 10%. DSC/TGA coupled with FTIR confirms the hydrocarbon evolution at ∼630 $K$ which coincides with the formation of $NiAl_3$ and $Ni_2Al_3$. Results from DSC/TGA measurements show that the concentration of hydrocarbon contaminants decrease with longer dry milling times, suggesting that the degree of contamination is affected by strain hardening during the dry milling treatment. Estimates of the degree of contamination are <0.05 wt.-% in all cases indicating that even low levels of contamination can significantly affect expansion of the product pellet.

The work also shows that initiating and consuming the kinetics and mechanics that produce the heat release of the first exothermc peak observed the DSC results has a significant effect on the combustion temperatures and in cold pressed MA Ni/Al green compacts. This was shown, by annealing 75% $t_{cr}$ MA Ni/Al milled at 403 and 460 $K$ for 30 $min$. X-ray diffraction data using Williamson-Hall analysis suggests that recovery occurs at an annealing temperature of 403 $K$ resulting in lower strains for both Al and Ni. At an annealing temperature of 460 $K$, both recovery and Al grain growth was observed along with the growth of $NiAl_3$ phase, which was also detected using scanning electron microscopy. The morphology and characteristic laminate dimensions, however, were not affected by the annealing. The annealing at 403 $K$ had little effect on combustion velocities and temperatures and were measured to be $\sim$16 $cm/s$ and $\sim$1840 $\pm$ 40 $K$ respectively. The annealing at 460 $K$ significantly reduced combustion velocities and temperatures down to $\sim$6 $cm/s$ and 1700 $\pm$ 30 $K$ respectively. The combustion temperatures were slightly under adiabatic temperatures calculated from heat of reactions measured from DSC analysis and were measured to be 1830 $\pm$ 30 $K$ for samples non-annealed and annealed at 406 $K$. Combustion temperatures for samples annealed at 460 $K$ were 1700 $\pm$ 40 $K$. These results show that the reaction front velocities and maximum temperatures are largely influenced by the formation of $NiAl_3$ during annealing, and that the strain relaxation due to annealing did not significantly affect the combustion behavior.

Lastly this work also shows that the processing control agents used to clean the milling jar for mechanical activation of metal-based reactives can have a large effect on the resulting material's properties and combustion characteristics. Cleaning with Hexanes, as opposed to water, decreases the amount of cold-welding on the milling jar walls and media during dry milling. The decreased cold-welding on the jar walls and milling media reduces the finial yield of fine particles ($<$106 $\mu m$) and increases the formation of solid solutions, intermetallics during milling. As a result of this heat release, combustion temperature, and combustion velocity decreases while the reaction onset temperature is not affected. The combustion temperature decreased

from $1830 \pm 30\ K$ to $1575 \pm 17\ K$ and the combustion velocities decreased from 16 $cm/s$ to 10 $cm/s$ for material milled in a hexane cleaned jar vs. a water cleaned jar.

# LIST OF REFERENCES

# LIST OF REFERENCES


[1] D. E. Eakins and N. N. Thadhani. Shock compression of reactive powder mixtures. *International Materials Reviews*, 54(4):181–213, 2009.

[2] E. B. Herbold, J. L. Jordan, and N. N. Thadhani. Observation of a minimum reaction initiation threshold in ball-milled ni + al under high-rate mechanical loading. *Journal of Applied Physics*, 109(6):066108–3, 2011.

[3] E. M. Hunt and M. L. Pantoya. Impact sensitivity of intermetallic nanocomposites: A study on compositional and bulk density. *Intermetallics*, 18(8):1612–1616, 2010.

[4] K. V. Manukyan, B. A. Mason, L. J. Groven, Y. C. Lin, M. Cherukara, S. F. Son, A. Strachan, and A. S. Mukasyan. Tailored reactivity of ni + al nanocomposites: Microstructural correlations. *Journal of Physical Chemistry C*, 116(39):21027–21038, 2012.

[5] A. R. Nair, B. A. Mason, L. J. Groven, S. F. Son, A. Strachan, and A. M. Cuitio. Micro-rve modeling of mechanistic response in porous intermetallics subject to weak and moderate impact loading. *International Journal of Plasticity*, 51(0):1–32, 2013.

[6] X. F. Zhang, A. S. Shi, J. Zhang, L. Qiao, Y. He, and Z. W. Guan. Thermochemical modeling of temperature controlled shock-induced chemical reactions in multifunctional energetic structural materials under shock compression. *Journal of Applied Physics*, 111(12):123501, 2012.

[7] E. M. Hunt, K. B. Plantier, and M. L. Pantoya. Nano-scale reactants in the self-propagating high-temperature synthesis of nickel aluminide. *Acta Materialia*, 52(11):3183–3191, 2004.

[8] E. M. Hunt and M. L. Pantoya. Ignition dynamics and activation energies of metallic thermites: From nano- to micron-scale particulate composites. *Journal of Applied Physics*, 98(3):034909–8, 2005.

[9] R. A. Yetter, G.t A. Risha, and S. F. Son. Metal particle combustion and nanotechnology. *Proceedings of the Combustion Institute*, 32(2):1819–1838, 2009.

[10] G. M. Fritz, S. J. Spey, M. D. Grapes, and T. P. Weihs. Thresholds for igniting exothermic reactions in al/ni multilayers using pulses of electrical, mechanical, and thermal energy. *Journal of Applied Physics*, 113(1):0149011–11, 2013.

[11] R. Knepper, M. R. Snyder, G. Fritz, K. Fisher, O. M. Knio, and T. P. Weihs. Effect of varying bilayer spacing distribution on reaction heat and velocity in reactive al/ni multilayers. *Journal of Applied Physics*, 105(8):0835041–9, 2009.

[12] J. Noro, A. S. Ramos, and M. T. Vieira. Intermetallic phase formation in nanometric ni/al multilayer thin films. *Intermetallics*, 16(9):1061–1065, 2008.

[13] J. C. Trenkle, L. J. Koerner, M. W. Tate, S. M. Gruner, T. P. Weihs, and T. C. Hufnagel. Phase transformations during rapid heating of al/ni multilayer foils. *Applied Physics Letters*, 93(8):0819031–3, 2008.

[14] G. H. Xu, K. F. Zhang, and Z. Q. Huang. The synthesis and characterization of ultrafine grain nial intermetallic. *Advanced Powder Technology*, 23(3):366–371, 2012.

[15] R. G. Xu, M. L. Falk, and T. P. Weihs. Interdiffusion of ni-al multilayers: A continuum and molecular dynamics study. *Journal of Applied Physics*, 114(16):1635111–7, 2013.

[16] A. Bacciochini, M. I. Radulescu, Y. Charron-Tousignant, J. Van Dyke, M. Nganbe, M. Yandouzi, J. J. Lee, and B. Jodoin. Enhanced reactivity of mechanically-activated nano-scale gasless reactive materials consolidated by cold-spray. *Surface and Coatings Technology*, 206(21):4343–4348, 2012.

[17] E. B. Herbold, J. L. Jordan, and N. N. Thadhani. Effects of processing and powder size on microstructure and reactivity in arrested reactive milled al plus ni. *Acta Materialia*, 59(17):6717–6728, 2011.

[18] B. A. Mason, L. J. Groven, and S. F. Son. The role of microstructure refinement on the impact ignition and combustion behavior of mechanically activated ni/al reactive composites. *Journal of Applied Physics*, 114(11):113501–7, 2013.

[19] A. Hadjiafxenti, I. E. Gunduz, C. C. Doumanidis, and C. Rebholz. Spark ignitable ball milled powders of al and ni at nial composition. *Vacuum*, 101(0):275–278, 2014.

[20] A. Hadjiafxenti, I. E. Gunduz, C. Tsotsos, T. Kyratsi, S. M. Aouadi, C. C. Doumanidis, and C. Rebholz. The influence of structure on thermal behavior of reactive al-ni powder mixtures formed by ball milling. *Journal of Alloys and Compounds*, 505(2):467–471, 2010.

[21] A. Hadjiafxenti, I. E. Gunduz, C. Tsotsos, T. Kyratsi, C. C. Doumanidis, and C. Rebholz. Synthesis of reactive al/ni structures by ball milling. *Intermetallics*, 18(11):2219–2223, 2010.

[22] R. V. Reeves, A. S. Mukasyan, and S. F. Son. Microstructural effects on ignition sensitivity in ni/al systems subjected to high strain rate impacts. In M. L. Elert, W. T. Buttler, J. P. Borg, J. L. Jordan, and T. J. Vogler, editors, *Shock Compression of Condensed Matter - 2011, Pts 1 and 2*, volume 1426 of *AIP Conference Proceedings*, pages 539–542. Amer Inst Physics, Melville, 2012.

[23] A. S. Rogachev, N. F. Shkodich, S. G. Vadchenko, F. Baras, D. Y. Kovalev, S. Rouvimov, A. A. Nepapushev, and A. S. Mukasyan. Influence of the high energy ball milling on structure and reactivity of the ni plus al powder mixture. *Journal of Alloys and Compounds*, 577:600–605, 2013.

[24] M. J. Cherukara, K. G. Vishnu, and A. Strachan. Role of nanostructure on reaction and transport in ni/al intermolecular reactive composites. *Physical Review B*, 86(7):075470, 2012.

[25] N. N. Thadhani. Shock-induced and shock-assisted solid-state chemical-reactions in powder mixtures. *Journal of Applied Physics*, 76(4):2129–2138, 1994.

[26] S. W. Du and N. N. Thadhani. Impact initiation of pressed al-based intermetallic-forming powder mixture compacts. *AIP Conference Proceedings*, 1195(1):470–473, 2009.

[27] R. V. Reeves, A. S. Mukasyan, and S. F. Son. Thermal and impact reaction initiation in ni/al heterogeneous reactive systems. *Journal of Physical Chemistry C*, 114(35):14772–14780, 2010.

[28] B. W. Asay, D. J. Funk, C. S. Fugard, P. M. Dickson, and B. F. Henson. Direct measurement of strain field evolution during dynamic deformation of an energetic material. *AIP Conference Proceedings*, 429(1):567–570, 1998.

[29] R. V. Reeves, J. D. E. White, A. M. Mukasyan, and S. F. Son. Comparison of mechanical and thermal ignition characteristics for reactivity enhanced ni/al powders. In M. L. Elert, W. T. Buttler, M. D. Furnish, W. W. Anderson, and W. G. Proud, editors, *Shock Compression of Condensed Matter - 2009, Pts 1 and 2*, volume 1195 of *AIP Conference Proceedings*, pages 466–469. 2009.

[30] M. A. Korchagin, T. F. Grigor'eva, B. B. Bokhonov, M. R. Sharafutdinov, A. P. Barinova, and N. Z. Lyakhov. Solid-state combustion in mechanically activated shs systems. i. effect of activation time on process parameters and combustion product composition. *Combustion, Explosion, and Shock Waves*, 39(1):43–50, 2003.

[31] C. Suryanarayana. Mechanical alloying and milling. *Progress in Materials Science*, 46(1-2):1–184, 2001.

[32] V. M. Maslov, I. P. Borovinskaya, and A. G. Merzhanov. Problem of the mechanism of gasless combustion. *Combustion, Explosion and Shock Waves*, 12(5):631–636, 1976.

[33] Y. S. Naiborodenko and V. I. Itin. Gasless combustion of metal-powder mixtures. *Combustion Explosion and Shock Waves*, 11(3):293–300, 1975.

[34] D. Y. Kovalev, N. A. Kochetov, and V. I. Ponomarev. Criteria of the critical state of the ni-al system during mechanical activation. *Combustion Explosion and Shock Waves*, 46(4):457–463, 2010.

[35] M. A. Korchagin, T. F. Grigor'eva, B. B. Bokhonov, M. R. Sharafutdinov, A. P. Barinova, and N. Z. Lyakhov. Solid-state combustion in mechanically activated shs systems. ii. effect of mechanical activation conditions on process parameters and combustion product composition. *Combustion, Explosion, and Shock Waves*, 39(1):51–58, 2003.

[36] A. Hadjiafxenti, I. E. Gunduz, T. Kyratsi, C. C. Doumanidis, and C. Rebholz. Exothermic reaction characteristics of continuously ball-milled al/ni powder compacts. *Vacuum*, 96(0):73–78, 2013.

[37] C. L. Yeh and W. Y. Sung. Combustion synthesis of ni3al intermetallic compound in self-propagating mode. *Journal of Alloys and Compounds*, 384(12):181–191, 2004.

[38] John J. Moore and H. J. Feng. Combustion synthesis of advanced materials: Part 1. reaction parameters. *Progress in Materials Science*, 39(45):243–273, 1995.

[39] S.H. Fischer and M.C. Grubelich. *A survey of combustible metals, thermites, and intermetallics for pyrotechnic applications*. 1996.

[40] A. Nouri and C. E. Wen. Surfactants in mechanical alloying/milling: A catch-22 situation. *Critical Reviews in Solid State and Materials Sciences*, 39(2):81–108, 2014.

[41] C. Mehta Somil, P. Somasundaran, X. Yu, and S. Krishnakumar. Colloid systems and interfaces stability of dispersions through polymer and surfactant adsorption. In *Handbook of Surface and Colloid Chemistry, Third Edition*, pages 155–196. CRC Press, 2008.

[42] Y. Wang, Z. K. Liu, and L. Q. Chen. Thermodynamic properties of al, ni, nial, and ni3al from first-principles calculations. *Acta Materialia*, 52(9):2665–2671, 2004.

[43] F. Cardellini, G. Mazzone, A. Montone, and M. Vittori Antisari. Solid state reactions between ni and al powders induced by plastic deformation. *Acta Metallurgica et Materialia*, 42(7):2445–2451, 1994.

[44] A. S. Mukasyan, B. B. Khina, R. V. Reeves, and S. F. Son. Mechanical activation and gasless explosion: Nanostructural aspects. *Chemical Engineering Journal*, 174(23):677–686, 2011.

[45] O. Politano, F. Baras, A. S. Mukasyan, S. G. Vadchenko, and A. S. Rogachev. Microstructure development during nial intermetallic synthesis in reactive ni-al nanolayers: Numerical investigations vs. tem observations. *Surface and Coatings Technology*, 215:485–492, 2013.

[46] P. Zhu, J. C. M. Li, and C. T. Liu. Adiabatic temperature of combustion synthesis of alni systems. *Materials Science and Engineering: A*, 357(12):248–257, 2003.

[47] L. Lu and M. O. Lai. *Mechanical Alloying*. Kluwer Academic Publishers, Boston, MA, 1998.

[48] A. Nouri, P. D. Hodgson, and C. E. Wen. Effect of process control agent on the porous structure and mechanical properties of a biomedical ti-sn-nb alloy produced by powder metallurgy. *Acta Biomaterialia*, 6(4):1630–1639, 2010.

[49] C. J. Rocha, R. M. L. Neto, V. S. Goncalves, L. L. Carvalho, and F. Ambrozio. An investigation of the use of stearic acid as a process control agent in high energy ball milling of nb-al and ni-al powder mixtures. In L. Salgado and F. A. Filho, editors, *Advanced Powder Technology Iii*, volume 416-4 of *Materials Science Forum*, pages 144–149. Trans Tech Publications Ltd, Stafa-Zurich, 2003.

[50] P. Ruuskanen and O. Heczko. Formation of amorphous fe1-xbx alloys during solid state alloying with hexane. *Journal of Non-Crystalline Solids*, 224(1):36–42, 1998.

[51] S. Srinivasan, S. R. Chen, and R. B. Schwarz. Synthesis of al/al3ti 2-phase alloys by mechanical alloying. *Materials Science and Engineering a-Structural Materials Properties Microstructure and Processing*, 153(1-2):691–695, 1992.

[52] V. S. Goncalvesa, C. J. Rocha, and R. M. L. Neto. Mechanical activation of nb75al powder mixtures with different process control agents. In L. Salgado and F. A. filho, editors, *Advanced Powder Technology VI*, volume 591-593 of *Materials Science Forum*, pages 160–167. Trans Tech Publications Ltd, Stafa-Zurich, 2008.

[53] A. Nouri, P. D. Hodgson, and C. Wen. Study on the role of stearic acid and ethylene-bis-stearamide on the mechanical alloying of a biomedical titanium based alloy. *Metallurgical and Materials Transactions a-Physical Metallurgy and Materials Science*, 41A(6):1409–1420, 2010.

[54] L. W. Deng, J. J. Jiang, S. C. Fan, Z. K. Feng, W. Y. Xie, X. C. Zhang, and H. H. He. Ghz microwave permeability of cofezr amorphous materials synthesized by two-step mechanical alloying. *Journal of Magnetism and Magnetic Materials*, 264(1):50–54, 2003.

[55] R. V. Reeves. *Control of Ignition and Reaction Behavior in Gasless Reactive Systems via Microstructural Modification*. PhD thesis, 2011.

VITA

# VITA

Benjamin Aaron Mason was raised in Los Alamos NM. After High School he attended Ricks College in Rexburg ID for one semester after which he served a two year full-time mission for the Church of Jesus Christ of Latter-Day Saints in Sao Paulo, Brazil. Upon returned to the United States attended Brigham Young University in Provo, UT where he earned a Bachelor's of Science degree in Mechanical Engineering. He then worked a Los Alamos National Laboratory for 9 months before commencing his graduate studies at Purdue University. Aaron earned his Masters of Science in Mechanical Engineering in 2010 and then went on to earn is Doctor of Philosophy in Dec of 2014 studying the combustion behavior of novel metal-based reactives. Upon graduation Aaron will continue his career as research in engineer with Schlumberger in Houston, TX.

LIST OF PUBLICATIONS

# LIST OF PUBLICATIONS

B. A. Mason, I. E. Gunduz, L. J. Groven, and S. F. Son. The Effect of Milling Media Cleaning Agent on the Mechanical Activation of Ni + Al. (manuscript in preparation).

B. A. Mason, I. E. Gunduz, L. J. Groven, and S. F. Son. Effect of Annealing on the Thermal Response and Combustion of Mechanically Activated Ni + Al Composite Powders. (manuscript in preparation).

B. A. Mason, T. R. Sippel L. J. Groven, I. E. Gunduz, and S. F. Son. Combustion Characteristics of Mechanically Activated Ni + Al Reactive Composites Tailored via Microstructural Refinement. (manuscript in preparation).

B. A. Mason, Lori J. Groven, and S. F. Son. The Role of Microstructure Refinement on the Impact Ignition and Combustion Behavior of Mechanically Activated Ni + Al Reactive Composites. *Journal of Applied Physics*, 114: 113501-7, 2013.

A. R. Nair, B. A. Mason, L. J. Groven, S. F. Son, A. H. Strachan, and A. M. Cuitio. Micro-RVE Modeling of Mechanistic Response in Porous Intermetallics Subject to Weak and Moderate Impact Loading. *International Journal of Plasticity*, 51: 1-32, 2013.

B. A. Mason, L. J. Groven, R. S. Yetter, and S. F. Son. Combustion Performance of Several Nanosilicon-based Nanoenergetic Composites. *Journal of Propulsion and Power*, 29 (6): 1435-1444, 2013.

K. V. Manukyan, B. A. Mason, L. J. Groven, Ya-Cheng Lin, M. Cherukara, S. F. Son, A. H. Strachan and A. S. Mukasyan. Tailored Reactivity of Ni + Al Nanocompoistes Microstructural Correlations. *Journal of Physical Chemistry*, 116 (39): 21027-21038, 2012.

B. A. Mason, J. M. Lloyd, S. F. Son, and B. C. Tappan. Burning Rate Studies of Bis-Triaminoguanidinium Azotetrazolate (TAGzT) and Hexahydro-1,3,5-trinitro-1,3,5-triazine (RDX) Mixtures. *Advancements in Energetic Materials and Chemical Propulsion*, Kenneth K. Kuo and Keiichi Hori editors, Begell House, 577-584, 2008.

D. E. Chavez, B. C. Tappan, B. A. Mason, and D. Parrish. Synthesis and Energetic Properties of Bis-(Triaminoguanidinium) 3,3-Dinitro-5,5-Azo-1,2,4-Triazolate (TAGDNAT): A New High-Nitrogen Material. *Propellants Explosives and Pyrotechnics*, 34: 475 479, 2009.